Geophysical Journal International

Geophys. J. Int. (2013) doi: 10.1093/gji/ggt197
Geophysical Journal International Advance Access published June 17, 2013

Palaeogeography of the Siberian platform during middle Palaeozoic Times (~450–400 Ma): new palaeomagnetic evidence from the Lena and Nyuya rivers

Vladislav Powerman,[1,2] Andrei Shatsillo,[1] Robert Coe,[3] Xixi Zhao,[3] Dmitry Gladkochub,[4] Robert Buchwaldt[5] and Vladimir Pavlov[1]

[1] *Schmidt Institute of Physics of the Earth, Russian Academy of Sciences, Moscow, Russia. E-mail: powerman@stanford.edu*
[2] *Department of Geological and Environmental Sciences, Stanford University, Stanford, CA, USA*
[3] *Department of Earth and Planetary Sciences, University of California, Santa Cruz, CA, USA*
[4] *Institute of the Earth's Crust, Russian Academy of Sciences, Irkutsk, Russia*
[5] *Department of Earth, Atmospheric and Planetary Sciences, Massachusetts Institute of Technology, Boston, Cambridge, MA, USA*

Accepted 2013 May 10. Received 2013 May 2; in original form 2012 September 18

SUMMARY

New reliable palaeomagnetic data from the Siberian platform help in deciphering its palaeogeography during ~450–400 Ma. Geochronology of late Devonian mafic sills provides time constraints for tectonic deformation along the southern margin of the Siberian Platform and thus a minimum age for the regional magnetic overprint. From a late Ordovician–Silurian sedimentary section of the Nyuya syncline in the southern part of the Siberian platform with the Devonian sills hosted nearby in early Palaeozoic sediments, pre-folding presumably primary magnetization was isolated from the sediments during stepwise thermal cleaning. High unblocking temperatures imply that haematite is the main carrier of magnetization. The sample-mean direction for 37 Ordovician samples from nine sites in stratigraphic coordinates is Ds = 168.5, Is = −5, ks = 22.3 and α_{95} = 5.1 and for 77 Silurian samples from six sites is Ds = 193.9, Is = 20.9, ks = 16 and α_{95} = 4.2. Another component recorded in both the Silurian and Ordovician samples is pre-folding, with a sample-mean direction of Ds = 204.4, Is = 37.9, ks = 27.2 and α_{95} = 2.7 for 104 samples from eight sites. This component was probably formed during a regional remagnetization event, which took place in post-early Silurian time. Putting this secondary component into a framework with available Palaeozoic data and geochronology further constrains its age to be early Devonian.

The isolated components yield new late Ordovician, early Silurian and early-middle Devonian palaeomagnetic poles. The revised middle Palaeozoic segment of the apparent polar wander path (APWP) for the Siberian platform provides new palaeogeographic constraints. Our data suggest that in late Ordovician the platform was situated in equatorial latitudes and was rotated 180° with respect to its present position. During middle-late Ordovician time, the platform did not experience any notable latitudinal drift. It started drifting to the north in the late Ordovician, and by the late Silurian it had travelled ~1500 km northwards and had rotated ~30° counter-clockwise (CCW). During late Silurian time, the platform continued northward drift and CCW rotation, and by the early Devonian it had drifted ~1100 km northwards and rotated 10° CCW relative to its Silurian position. After that, the rotation of the platform changed to clockwise (CW), and by the late Devonian had drifted another 1500 km to the north and had rotated ~60° CW.

We evaluated palaeomagnetically viable positions from 450–400 Ma of the three largest Laurasian cratons, Siberia, Baltica and Laurentia, based on the new data and previously published APWPs. Contrary to several published reconstructions, the Siberian platform could not have been situated to the north of the Caledonian suture in mid-Silurian time, but was probably located either at the eastern or the western side of Laurussia. The new data are compatible with an early Devonian position of Siberia similar to the modern Eurasian configuration. They also support the post- early or middle Devonian relative rotation between the Aldan and Angara blocks of the Siberian platform.

Key words: Palaeomagnetism applied to tectonics; Palaeomagnetism applied to geologic processes; Remagnetization; Cratons; Asia.

INTRODUCTION

Eastern Eurasia makes up a broad region of active plate tectonics and intracontinental deformation. It is dominated by large continental blocks of Siberia, Sino-Korea, Yangtze, Tarim and India as well as large composite regions of smaller blocks and accreted terranes comprising Tibet, Mongolia (Outer and Inner), Kazakhstan and the Central Asiatic Orogenic Belt (CAOB) (Fig. 1). The formation of this collage has a long history, commencing in the late Precambrian with the accretion of the island arcs of central Asia that continued well into the Palaeozoic and Mesozoic (Zonenshain *et al.* 1990; Xiao *et al.* 2003; Windley *et al.* 2007).

Despite long-term international effort, some of the major geological and tectonic events that led to the assemblage of Eurasia are still poorly understood. This is especially true for the Siberian platform (Fig. 1). Although the palaeogeography of the Siberian platform is fairly well known for certain age intervals, such as the middle Cambrian–middle Ordovician and around the Permian–Triassic boundary, there are many long gaps in the history of this old craton, introducing significant uncertainties into global tectonic reconstructions. One such gap for the Siberian platform is in the middle Palaeozoic.

There are several different geological approaches for estimating palaeogeography. Palaeomagnetism is one of the most quantitative and reliable methods, providing key information for quantifying the motions of crustal blocks, especially prior to the formation of the oldest surviving seafloor crust. In the middle Palaeozoic, most of published reconstructions (e.g. Cocks & Torsvik 2002; Golonka *et al.* 2006; Lawver *et al.* 2011) are based on positions of the Siberian platform derived from interpolation between early and late Palaeozoic palaeomagnetic poles.

In this study, we address the deficiency of middle Palaeozoic palaeomagnetic data for the Siberian platform by presenting new results from Ordovician–Devonian rocks from the southern margin of Siberian platform. The area was chosen based on the presence of palaeomagnetically promising rocks (red- and green-coloured beds), the absence of heavy tectonic deformation and the favourable location away from voluminous Permian–Triassic traps—a potent source of magnetic overprints. Our pilot data (Shatsillo *et al.* 2007) allowed us to formulate initial hypotheses for the palaeogeography of the Siberian platform during Silurian and early Devonian. In this study, we have conducted detailed palaeomagnetic and geochronologic analyses for late Ordovician–late Devonian rocks that validate those hypotheses and expand the time frame.

GEOLOGICAL SETTINGS

Tectonic framework

The study area is located at the southern edge of the Siberian platform, northwards from the Patom fold-and-thrust belt (Fig. 1). Patom Belt was developed on the Siberian Proterozoic passive margin and is a northern segment of the larger CAOB. The CAOB formed mainly in the Palaeozoic during the closure of Palaeo-Asian Ocean, which separated Baltica from Siberia, and Siberia from Tarim and Sino-Korea (Khain 2001).

The southern part of the Siberian platform consists of crystalline basement (not exposed in the vicinity) and Neoproterozoic–Palaeozoic sedimentary cover. The tectonics of the study area is characterized by shallow folds: large Ordovician–Silurian cored synclines and few narrow anticlines cut by low-amplitude northwestward verging thrust faults. Their amplitudes rapidly decrease towards the platform's centre. These minor folds and thrusts in the study area are concordant with those within the Patom Belt, and thus were probably caused by the same orogenic events (DeBoisgrollier *et al.* 2009; Nikishin *et al.* 2010). The timing of folding in the area is constrained by the youngest folded rocks—late Devonian mafic sills of Zharov complex (DeBoisgrollier *et al.* 2009; M. Tomshin, personal communication, 2008), and less confidently, by Permian to Carboniferous post-tectonic granitoids of the Angara–Vitim batholith (Tsygankov *et al.* 2007) that truncate both the sediments and the thrust faults of the Patom Belt to the south. Dating of two of the folded mafic sills places new constraints on the age of deformation.

The study area is located within a large tectonic structure—the Nyuya syncline (Figs 1 and3), which is located far from the front of the Patom orogen and is characterized by minor fold-and-thrust deformation. Sedimentary beds of the syncline have gentle dips, not exceeding 10° (see, e.g. Fig. 2). The Nyuya syncline occupies approximately 6000 km^2 in map view (Fig. 3), with its hinge plunging shallowly to the southwest. Silurian sediments occur in the cores of synclinal folds, Cambrian and middle Ordovician sediments form the limbs, and all are unconformably overlain by relatively flat and undeformed early Jurassic sediments. The Ordovician and Cambrian sediments of the Nyuya syncline host several Zharov Complex mafic sills, which can be traced for long distances are folded together with the host sedimentary rocks, repeating the overall tectonic structure of the area (Figs 3 and 4).

Stratigraphy of the study region

The sedimentary rocks in the study region overlie the crystalline basement of the Siberian platform (not exposed, Parfenov 2001). They cover a wide interval from late Proterozoic (including Ediacaran) to Jurassic with few minor unconformities and a major Devonian–Triassic hiatus (Fig. 3). The section starts with a late Precambrian siliciclastic and carbonate succession, which is only exposed in the cores of anticlines and consists of three sedimentary groups, Dalnetaiginskaya, Zhuinskaya and Bodaibinskaya. Precambrian sediments are overlain by the lower middle Cambrian carbonates, which are covered by upper Cambrian clastics. The overlying lower middle Ordovician is characterized by the dominance of

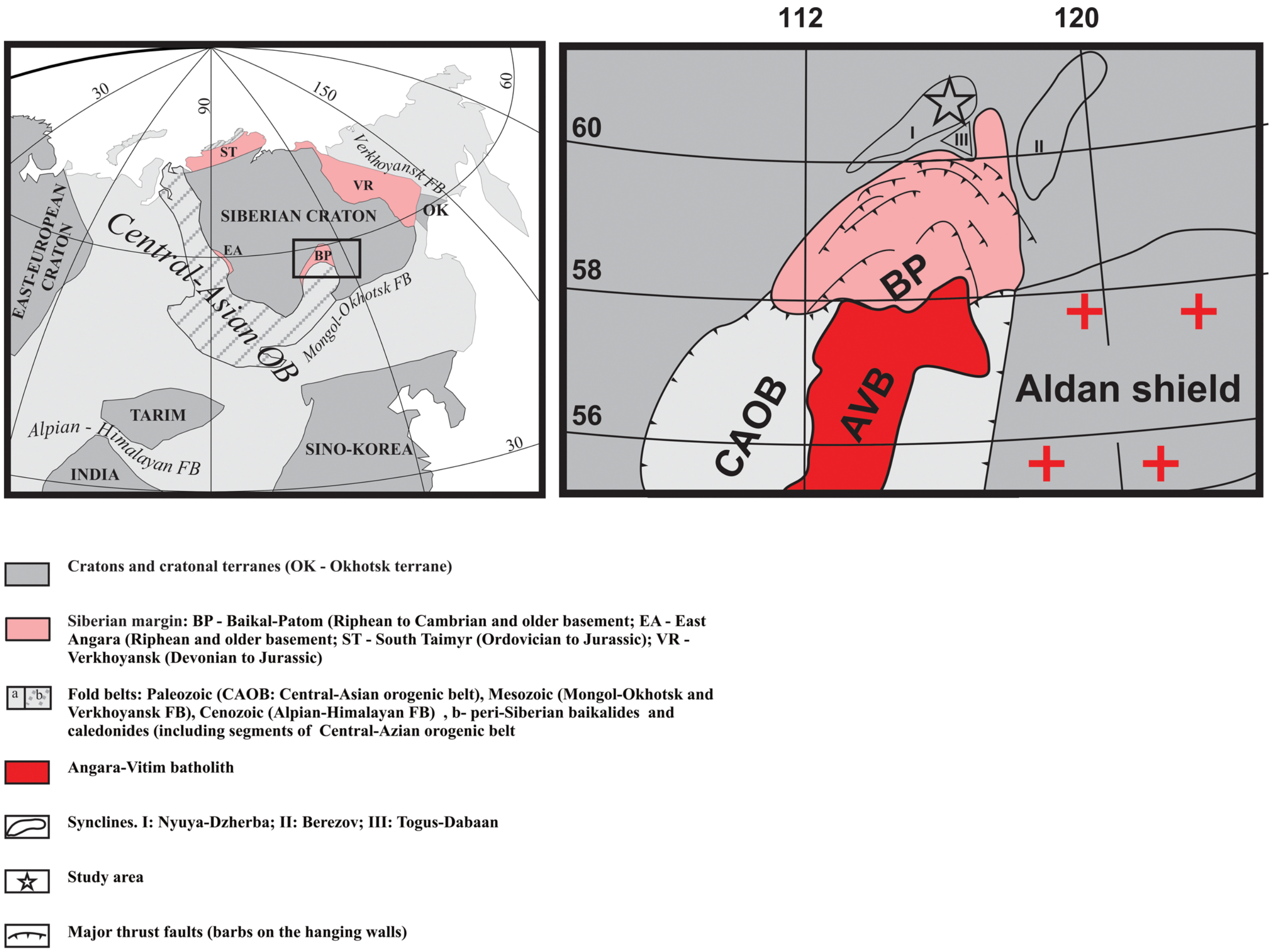

Figure 1. Left-hand panel: Simplified tectonic map of Asia showing major cratons and foldbelts. Right-hand panel: Simplified tectonic map of the southern part of the Siberian platform.

carbonates. The studied part of the sedimentary section starts with mudstone and siltstone red beds belonging to the late Ordovician Krasnokamenskaya formation. 'Drepanodistacodus victrix Mosk.' and 'Acanthodina regalis Mosk.' conodonts (Table A1 in Appendix A) constrain its depositional age to the Caradoc–Ashgill epochs of late Ordovician (Berger *et al.* 2007). A minor unconformity separates late Ordovician and early Silurian sediments. The Silurian section starts with the 60-m thick Melichanskaya formation. 'Distomodus kentuckyensi' conodont fossils place Melichanskaya formation in the early Silurian Llandovery epoch (Table A1). The Melichaskaya formation is conformably overlain by the 65-m thick Utakanskaya formation. Both the Melichanskaya and Utakanskaya formations are dominated by grey-coloured marls, interbedded with red siltstones and mudstones. The Utakanskaya formation is conformably overlain by the 15-m thick Nyuskaya formation, which is entirely confined to the Silurian Wenlockian stage (S_1) based on palaeontology (Table A1), and is overlain by the 50-m thick Neryukteiskaya formation, which is devoid of fossils.

Berger *et al.* (2007) assign a Ludlowlian age to the Neryukteiskaya formation based on its conformable relationship with the underlying Nyuskaya formation. The Proterozoic–Palaeozoic sedimentary section is unconformably overlain by flat and undeformed early Jurassic sediments, which are the youngest rocks in the area aside from Quaternary alluvium.

SAMPLING AND METHODS

Sampling

We have collected palaeomagnetic samples from the Ordovician and Silurian Krasnokamenskaya, Melichanskaya and Utakanskaya (undivided) and Neryukteiskaya formations. No samples from the Nyuskaya formation were collected due to the absence of red and green beds, which usually carry a strong palaeomagnetic signal. The total thickness of the sampled interval is approximately 200 m.

The Krasnokamenskaya formation was sampled in two outcrops along the shore of Nyuya River (outcrops 62 and 65; Fig. 3 and Table 1), spaced approximately 30 km apart. Each outcrop was divided into five sites located sequentially from the base to the top of each section and six samples were collected from each site, making a total of 60 samples. The Melichanskaya and Utakanskaya formations were sampled together at nine outcrops on the Nyuya River and one outcrop on the Lena River. Outcrops were spaced 5 km apart on average and 247 samples were collected. The Neryukteiskaya formation was sampled in one outcrop on the Lena River (L1) and 23 samples were collected. In all cases, hand blocks were gathered. They were oriented with a magnetic compass, which was entirely adequate given the low magnetic susceptibility values of the rocks.

Sills of the Zharov complex were also sampled for palaeomagnetic purposes. The magnetic record of the sills turned out to be not

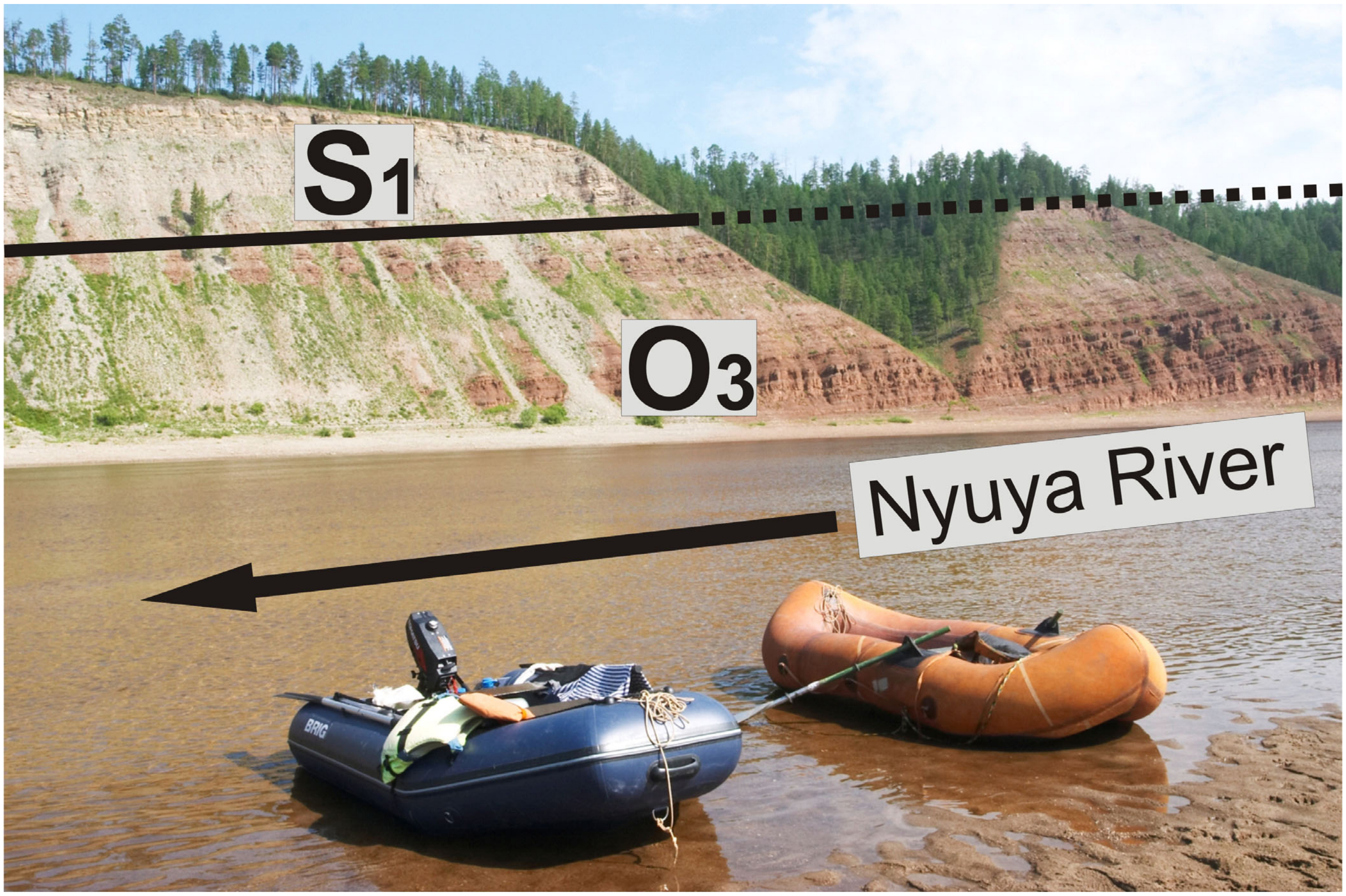

Figure 2. Photograph of the contact between Upper Ordovician silt- and mudstones and lower Silurian marls at the right bank of Nyuya River. Flow direction is indicated with an arrow.

easily interpretable, thus it won't be discussed in this publication. The geochronology of the sills, however, resulted in a better understanding of the age of the folding, which in turn constrained the age of magnetization. We collected two geochronology samples from two folded mafic sills hosted in the lower Ordovician sediments (Figs 3 and 4; Table 1). Sample VP-VII-Mu-1 is from a sill that can be traced for more than 8 km on the geological map (Nikolsky & Kavelin 1984), and has a thickness varying from 80 to 30 m. At our sampling location at the right bank of Lena River, directly across from the mouth of Nyuya River, this sill was at its thinnest.

Sample VP-VI-Le-1 was collected from another sill, hosted in lower Cambrian limestones (Figs 3 and 4) that structurally constitute the eastern limb of the Togus–Dabaan syncline. Both sills are gabbro-dolerites and consist of plagioclase (50 per cent), augite (40 per cent), olivine (5 per cent), titanomagnetites and accessory minerals including apatites and zircons. Plagioclases and olivines are altered and replaced by low-grade metamorphic minerals (serpentines, epidotes, calcites and iddingsites).

Laboratory procedures

Oriented hand samples were cut into cubic specimens with 1–2 cm sides. Directions and intensities of the natural remanent magnetization (NRM) were measured using horizontally and vertically oriented 2G three-axis cryogenic magnetometers in the Palaeomagnetic Laboratories at the University of California Santa Cruz (USA), and Ludwig-Maximilians University (Munich, Germany), respectively. All samples were subjected to stepwise thermal demagnetization experiments until complete destruction of NRM, sometimes reaching maximum temperatures of 680 °C. The magnetometers, as well as the furnaces used for thermal demagnetization (Schoenstedt TSD-1 in Munich, and custom-designed thermal demagnetizer at UC Santa Cruz) experiments, were housed in magnetically shielded rooms. The demagnetization results were analysed using orthogonal vector plots and stereographic projections. Linear and planar elements in the demagnetization data were identified by eye and subjected to principal component analysis (Kirschvink 1980).

PALAEOMAGNETIC RESULTS

Late Ordovician

Late Ordovician samples are characterized by moderate- to good-quality palaeomagnetic signals. More than half of the samples yielded interpretable results. Values of NRM vary between 5×10^{-4} and 5×10^{-3} A m^{-1}. Three NRM components were isolated in late Ordovician samples.

A low-temperature component LT_o ('LT'—low temperature, 'o'—Ordovician; same naming strategy is used throughout the text) coincides with the Earth's present magnetic field, indicating its recent, probably viscous, origin. LT was destroyed after the first few heating steps.

The direction of a single-polarity middle-temperature component MT_o does not coincide with the modern magnetic field. MT_o is an intermediate component, since it does not decay towards the origin of vector component diagrams (Fig. 5). The term

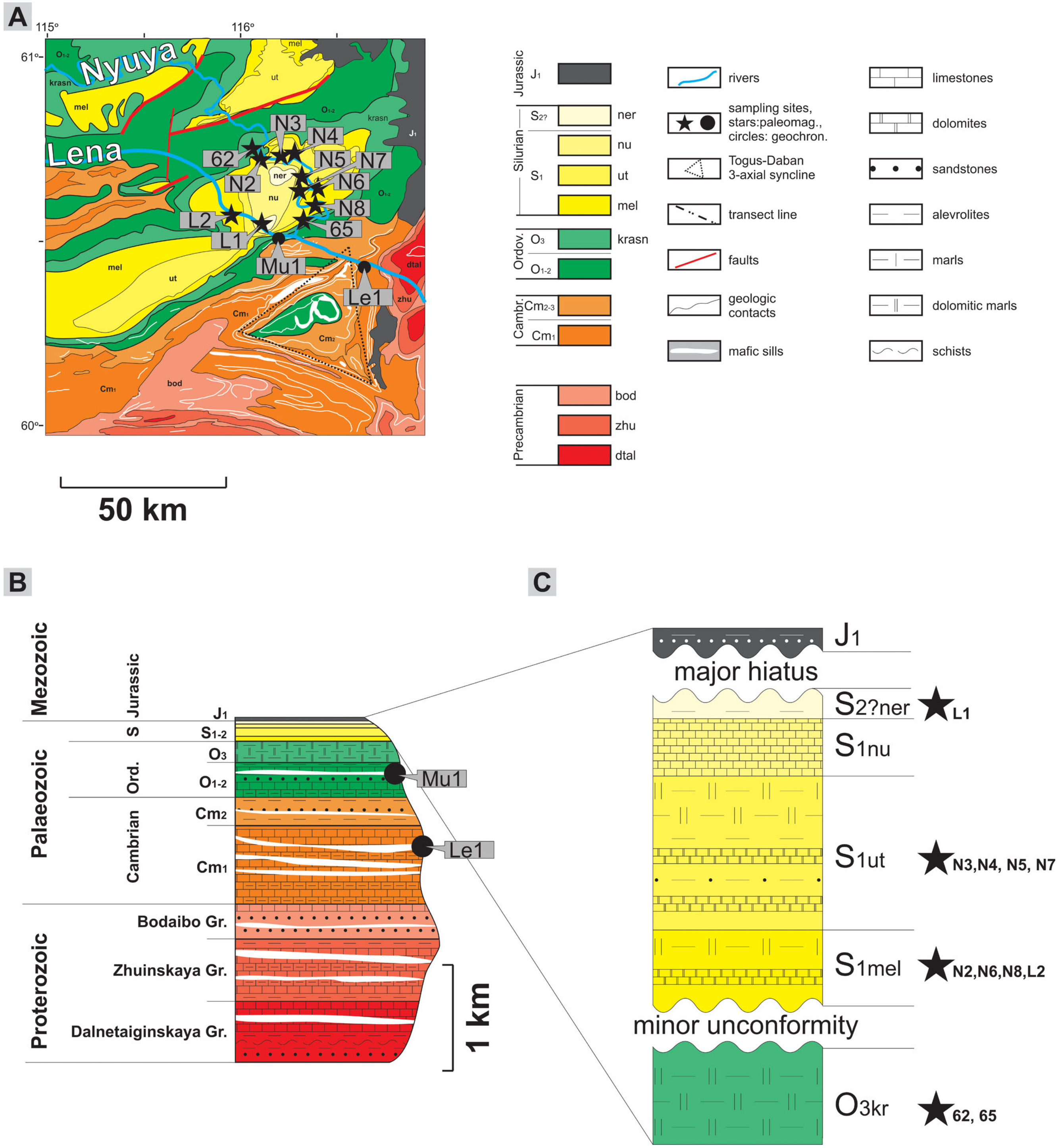

Figure 3. Geology of the study area. (a) geological map, compiled after 1:200 000 state geological maps. (b) A generalized stratigraphic column. The positions of sampled sills are shown. (c) Late Ordovician–early Jurassic segment of the stratigraphic column. Sampled formations are marked with stars; numbers correspond to the sampling sites (Table 1). Geochronology sampling site names are shortened (Mu1 instead of VP-VII-Mu-1 and Le1 instead of VP-VI-Le-1).

'middle-temperature' is used conditionally, because in some instances its maximum unblocking temperatures were as high as 640 °C. However, in the majority of cases this component was destroyed in the range of 400–500 °C. MT_o was isolated in 30 samples from nine sites. 3–10 demagnetization steps (six on average) were used to calculate the direction of the component in each sample. The direction-correction (DC) fold test by Enkin (1994) yields an inconclusive result for sample-mean MT_o. However, after combining MT_o with a middle-temperature component from Silurian samples (MT_s), the DC test yielded a positive result. Inconclusive test results of MT_o are most likely explained by insufficient statistical sampling and by minor bedding variations between sites.

The third, high-temperature component HT_o is characterized by single polarity and highest overall unblocking temperatures in the

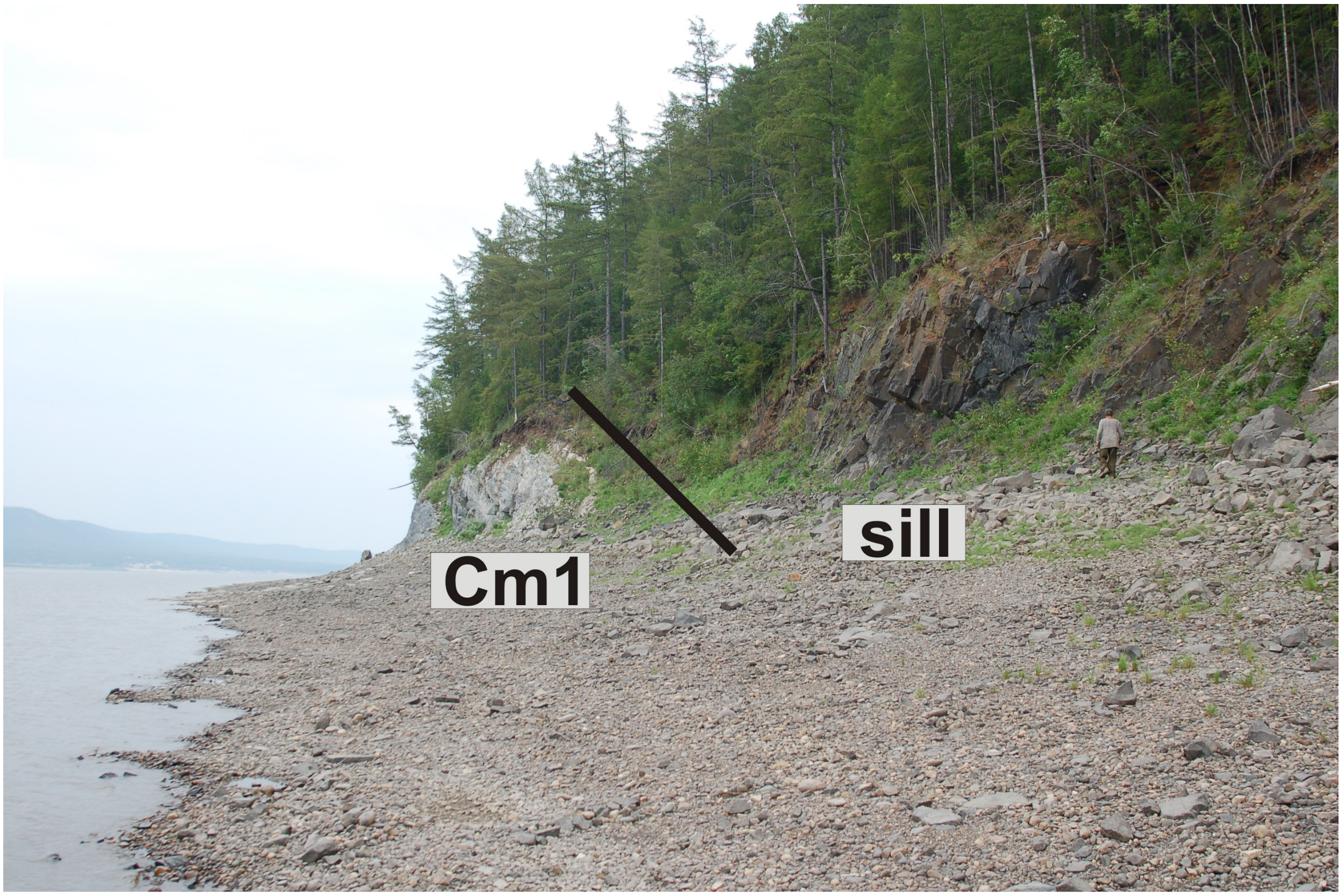

Figure 4. Photograph of the lower contact of the sampled sill (VP-VI-Le-1) with Cambrian limestones at the right shore of Lena River. Approximate position of the unexposed contact is shown with a line.

Table 1. Sampling locations. See Fig. 3 for the stratigraphic positions of sites.

Site	Latitude (N)	Longitude (E)	Description
		Geochronology sites	
VP-VII-Mu-1	60°31′14.8″	116°17′9.1″	Gabbro-dolerite hosted in O_2 sediments
VP-VI-Le-1	60°26′33.9″	116°39′53.3″	Gabbro-dolerite hosted in cm_1 sediments
		Palaeomagnetic sites	
N2	60°43′41.3″	116°9′48.8″	Dolomitic marls, dolomites, siltstones
N4	60°43′31.2″	116°18′38.1″	
N6	60°38′46.7″	116°25′34.0″	
N7	60°38′17.8″	116°20′33.4″	
N8	60°36′13.14″	116°26′38.28″	
L1	60°34′3.19″	116°7′47.29″	
L2	60°36′18.34″	115°54′48.74″	
62	60°44′38.33″	116°7′35.83″	
65	60°34′30.12″	116°23′44.04″	

range of 440–675 °C. HT_o always decayed towards the origin of vector component diagrams (Fig. 6). This property was the determining characteristic for the isolation of components. Three to nine demagnetization step directions (seven on average) were used to calculate this component. Results for HT_o were obtained from nine of 10 sampled sites (site #65/4 contained only one sample with stable remanence, interpreted as HT_o, so it was excluded from statistical count). Direction distributions are shown in Fig. 11, and site-mean and sample-mean palaeomagnetic directions from HT_o component are listed in Table 2. In both cases, DC fold tests yielded positive results, suggesting a pre-folding age of magnetization. We used a sample-mean direction for calculating the corresponding palaeomagnetic pole (#8 in Table 5).

Early Silurian Melichanskaya and Utakanskaya formations (undivided)

Samples from the Melichanskaya and Utakanskaya formations (undivided) possessed a moderate- to poor-quality palaeomagnetic signal. 135 out of 209 studied samples were used to isolate the component. The rest of the samples carried a weak signal that could not be interpreted. NRM values vary between 2×10^{-5} and

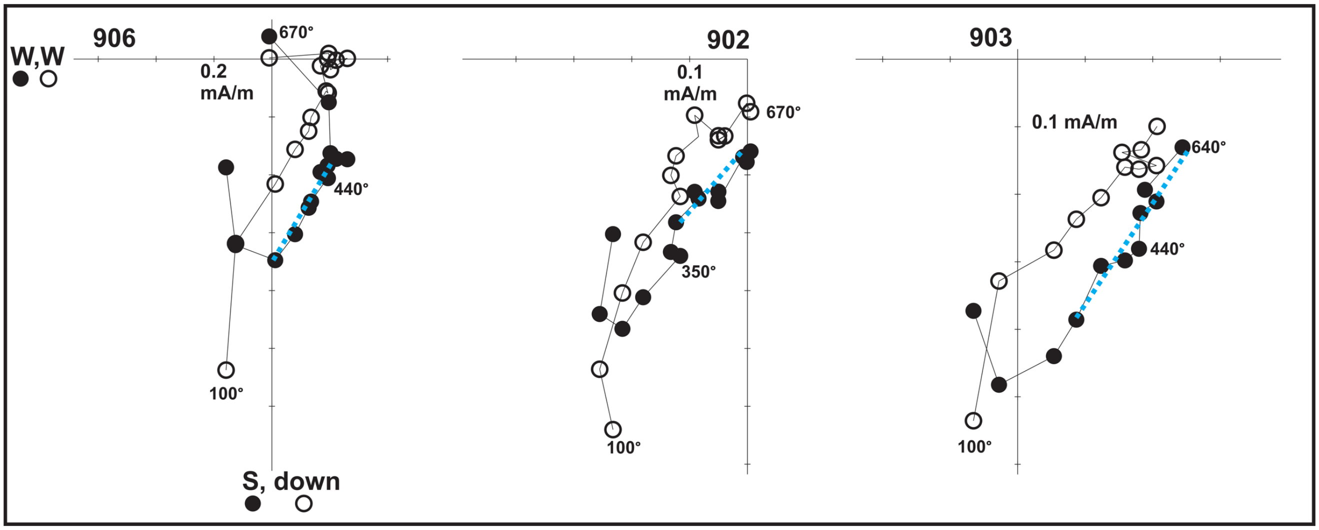

Figure 5. Orthogonal projection of the results of stepwise thermal demagnetization of Ordovician (Krasnokamenskaya formation) samples containing middle-temperature (MT_o) component (shown with dotted lines). Stratigraphic coordinates are used for data projection.

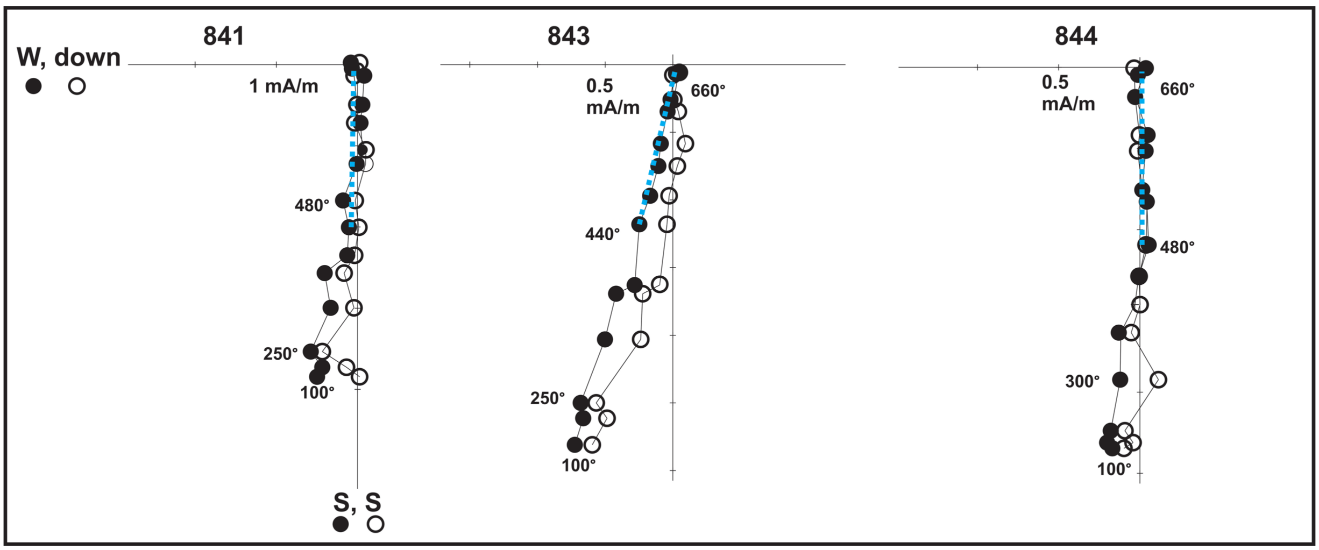

Figure 6. Thermal demagnetization results of representative Ordovician samples that contain high-temperature (HT_o) components. We have chosen a different orthogonal projection here for better demonstration of the isolated component. Stratigraphic coordinates are used.

4×10^{-3} A m^{-1}. The character of vector component diagrams was similar to that of the Ordovician samples. Aside from a low-temperature viscous component, two other components, middle- and high- temperature ones, were isolated.

A single-polarity middle-temperature component MT_s was isolated in 73 samples from six sites (L2, N2, N4, N6, N7 and N8). Again, we considered missing the origin on orthogonal projections (Fig. 7) as the determining characteristic to isolate the component. Unblocking temperatures of MT_s lay in a wide range (350–640 °C). 3–15 (six on average) demagnetization steps were used to isolate the component. The average direction of the MT components did not differ statistically from those of MT_o (see Table 3; statistical algorithm discussed in McFadden & McElhinny (1990)). This allowed us to join them and deal with a sole middle-temperature (MT) component. The combined sample-mean MT component was calculated using six Silurian sites (L2, N2, N4, N6, N7 and N8) and two Ordovician outcrops (62 and 64). As noted above, the combined MT component successfully passes the DC fold test. The corresponding palaeomagnetic pole (#15) is presented in Table 5.

A high-temperature component $HT_{s(mel+ut)}$ (Figs 8 and 9) of dual polarity was isolated in 54 samples from five sites: L2, N2, N4, N7 and N8. Decay towards the origin was the determining property for the identification and isolation of components. The unblocking temperatures of HT lay in the range of 520–675 °C and $HT_{s(mel+ut)}$ had maximum unblocking temperatures at or near the Curie temperature of haematite (T_c = 675 °C) in the majority of samples. 3–16 (seven on average) demagnetization steps were used to isolate HT in each sample. The DC fold test and reversal test both yielded inconclusive results for the $HT_{s(mel+ut)}$ component. Its average direction was statistically different from HT_o and MT (Table 4).

Late Silurian Neryukteiskaya formation

Samples from the Neryukteiskaya formation possessed a rather strong palaeomagnetic signal characterized by a single high-temperature (HT) component (Figs 10 and 11). The clustering of directions was remarkably tight. Magnetization values were the

Table 2. Characteristic magnetization components. *N*, number of samples, D, declination, I, inclination, $\alpha95$ and K, statistical characteristics of the Fisher distribution. Index 'g' indicates geographical coordinate system, 's', tilt-corrected stratigraphic coordinates. Fold test results (DC) and calculated palaeomagnetic poles are shown.

sites	estimate of magnetization's age	N	Dg	Ig	Kg	a95g	Ds	Is	Ks	a95s	DC test results	Pmag pole
High temperature component in Krasnokamenskaya fm. of Upper Ordovician (Hto)												
62/1	Late Ordovician, Caradoc-Ashgill	6	172.5	-4.4	101	6.7	173.1	-6.4	105	6.6		
62/2		4	172.4	-2.8	18.3	22	172.6	-4.5	18.3	22.1		
62/3		4	170.5	-6.5	153	7.4	171	-7.4	151	7.5		
62/4		5	165	0.4	54.2	11	165	-0.1	53.7	10.5		
62/5		4	177.7	-11.5	31.4	17	178.6	-11.4	31.3	16.7		
Site-mean, outcrop 62		5 sites (23 samples)	171.6	-5	163	6	172	-6	163	6	Inconclusive, DC slope = 0.405+/- 9.366	
65/1		4	143	-8.1	15.4	24	143	6.3	15.4	24.1		
65/2		4	176.9	-24.1	12.2	27	175.5	-9.7	12.3	27.3		
65/3		4	166.9	-18.6	17	23	166.5	-3.7	17	23		
65/5		3	156.7	-17.2	25.5	25	156.7	-2.2	25.5	24.9		
Site-mean, outcrop 65		4 sites (15 samples)	160.5	-17.4	28	18	160.4	-2.4	28	17.7	Inconclusive, DC slope = 0.537+/- 8.148	
Site-mean, outcrops 62 and 65		9 sites (38 samples)	166.9	-10.5	36.1	8.7	166.9	-4.4	44.4	7.8	Positive, DC slope =0.735+/- 0.564	
Sample mean, outcrops 62 and 65		**37**	**168.5**	**-10.3**	**19.6**	**5.5**	**168.5**	**-5**	**22.3**	**5.1**	**Positive, DC slope =0,833+/- 0,536**	**plat=-31.3; plong=129.5; dp/dm=2.6/5.1; a95=3.6**
Middle temperature component in Ordovician rocks (Mto)												
Outcrop 62 (sites 62/2-62/5)	Early Devonian (?)	12	191.2	24.6	88.5	4.6	188.7	26	87	4.7		
Outcrop 65 (sites 65/1-65/5)		18	200.8	23.4	31.5	6.3	206.7	34	31.5	6.3		
Sample-mean, outcrops 62 and 65		31	203.7	28.8	21.7	5.7	207.6	36.5	20.3	5.9	Inconclusive, DC slope =-0.110+/- 0.958	
High temperature component in Silurian rocks												
Early Silurian Melichanskya + Utakanskaya fms., HTs(mel+ut), Nyuya River												
Sample-mean, sites N2, N4, N7, N8	S_1	28	194.9	29.5	7.5	11	194.8	24.2	7.3	10.8		
Melichanskya fm., HTs(mel), Lena River												
L2	S_1	26	193.4	23.3	28.1	5.4	194	21.4	31.9	5.1		
Melichanskya + Utakanskaya fms., HTs(mel+ut), Lena + Nyuya Rivers												
Sample-mean, sites L2, N2, N4, N7, N8	S_1	54	194.1	26.4	11.6	6	194.4	22.8	11.8	5.9	Inconclusive, DC slope =-0.792 +/- 1.148	
Late Silurian, HTs(ner) Neryukteiskaya fm.												
L1	S_2	23	194.3	12.3	182	2.2	192.9	16.7	139	2.6		
Early-Late Silurian, HTs Melichanskya + Utakanskaya + Neyukteiskaya fms												
Sample-mean, sites L1, L2, N2, N4, N7, N8	$S_{1\text{-}2}$	**77**	**194.2**	**21.9**	**14.7**	**4.4**	**193.9**	**20.9**	**16**	**4.2**	**Positive, DC slope = 1,145+/- 0,637**	**plat=-17.6; plong=102.0; dp/dm=2.3/4.4; a95=3.2**

Table 2 (*Continued.*)

sites	estimate of magnetization's age	N	Dg	Ig	Kg	a95g	Ds	Is	Ks	a95s	DC test results	Pmag pole
Middle temperature component in Early Silurian sediments (MTs)												
L2	Early Devonian (?)	31	202.2	34.6	37.4	4.3	202.2	32.4	34.9	4.4		
N2		9	206	44.5	19.7	12	201.9	41.3	23.4	10.9		
N4		7	206.1	40.4	40.7	9.6	203.8	33.2	49.7	8.6		
N6		4	229	39.1	114	8.6	229	39.1	114	8.6		
N7		10	195.7	37.6	42	7.5	200.2	34.4	42	7.5		
N8		10	209.1	39.7	23	10	209.5	36.6	23.4	10.2		
Site-mean, sites L2, N2, N4, N6, N7, N8		6 sites (71 samples)	207.9	39.8	75.9	7.7	207.5	36.6	76	7.7	Inconclusive, DC slope =-0.499+/-1.715	
Sample-mean, sites L2, N2, N4, N6, N7, N8		73	204.3	38.2	29.3	3.1	204.2	35.4	29.5	3.1	Inconclusive, DC slope =-0.533+/-0.381	
Middle temperature component in early Silurian and Ordovician rocks (MT)												
Site-mean, sites 62, 64, L2, N2, N4, N6, N7, N8	**Early Devonian (?)**	8 sites (104 samples)	204.5	36	46.6	8.2	204.8	35.1	61.3	7.1	Positive, DC slope = 0.943+/-0.349	plat=-7.5; plong=92.8; dp/dm=4.7/8.2; a95=6.2
Sample-mean, 62, 64, L2, N2, N4, N6, N7, N8		**104**	**204**	**37.5**	**22.6**	**3**	**204.4**	**37.9**	**27.2**	**2.7**	**Positive, DC slope = 0.967+/-0.302**	**plat=-5.9; plong=93.2; dp/dm=1.9/3.2; a95=2.5**

Note: Bold values are used to calculate palaeomagnetic poles.

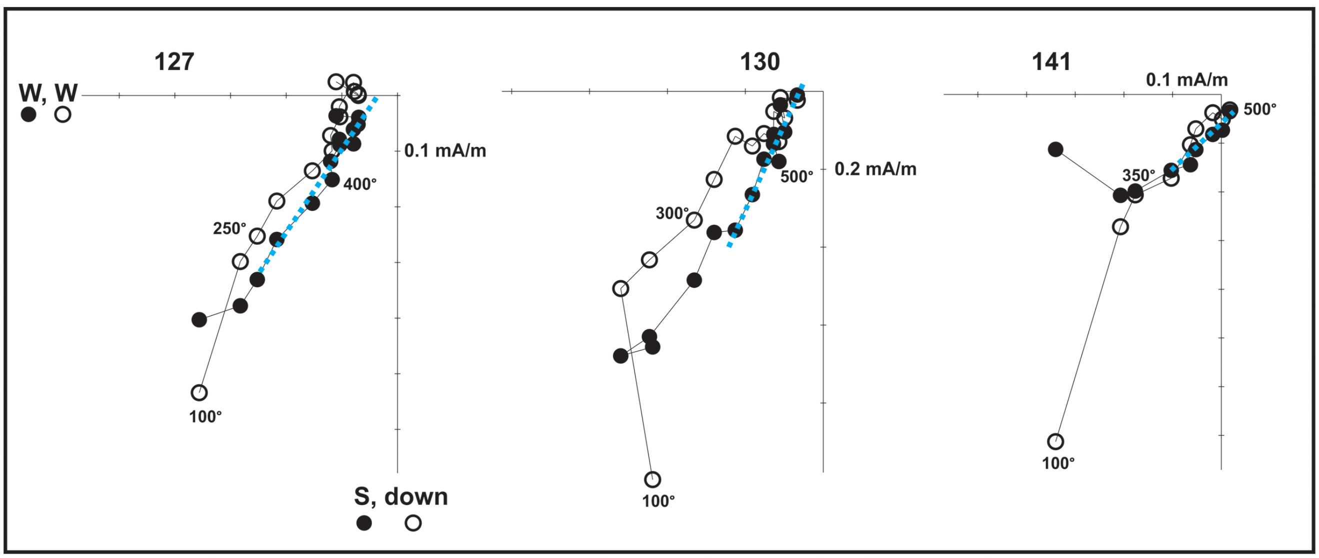

Figure 7. Thermal demagnetization results of representative early Silurian (Melichanskaya + Utakanskaya formations) samples that contain middle-temperature (MT_s) component. Stratigraphic coordinates are used.

Table 3. Statistical comparison of isolated palaeomagnetic directions: angles between palaeomagnetic directions/critical angles (employed algorithm is discussed in McFadden & McElhinny (1990)). Values that do not differ statistically are shown in bold.

	HT_o	HT_s	**MT**	MT_o	MT_s	$HT_{s(mel+ut)}$	$HT_{s(ner)}$
HTo	–	36.6°/6.3°	53.2°/10.1° (sites); 53.2°/3.6° (samples)	56.1°/6.4°	53.0°/4.9°	38.2°/7.4°	33.2°/4.9°
HT_s	–	–	17.1°/4.1°	19.6°/7.5°	17.1°/5.2°	–	–
MT	–	–	–	–	–	13.9°/6.5°	21.2°/4.0°
MT_o	–	–	–	–	**3.0°/6.1°**	16.5°/11.8°	23.7°/7.0°
MT_s	–	–	–	–	–	15.2°/6.2°	21.2°/5.7°
$HT_{s(mel+ut)}$	–	–	–	–	–	–	**6.3°/8.9°**
$HT_{s(ner)}$	–	–	–	–	–	–	–

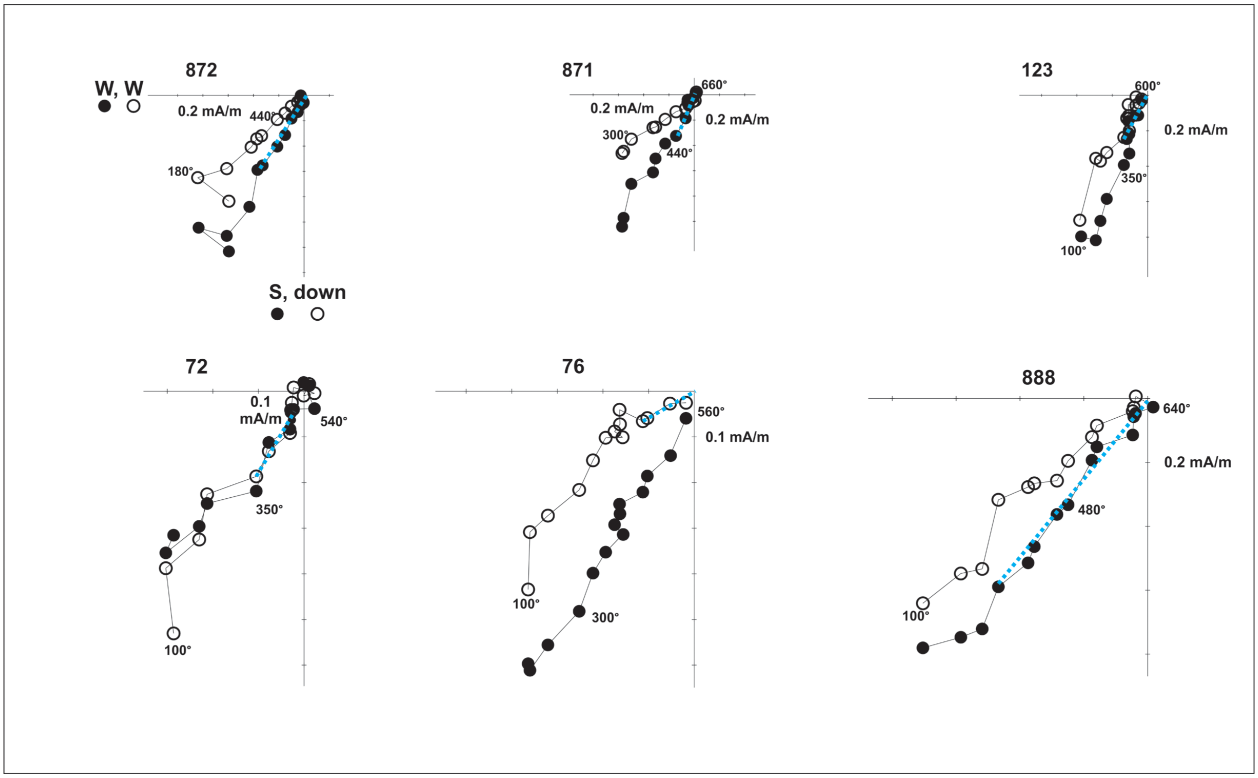

Figure 8. Thermal demagnetization results of representative early Silurian samples that contain high-temperature (HT_S) components of normal polarity. Stratigraphic coordinates are used.

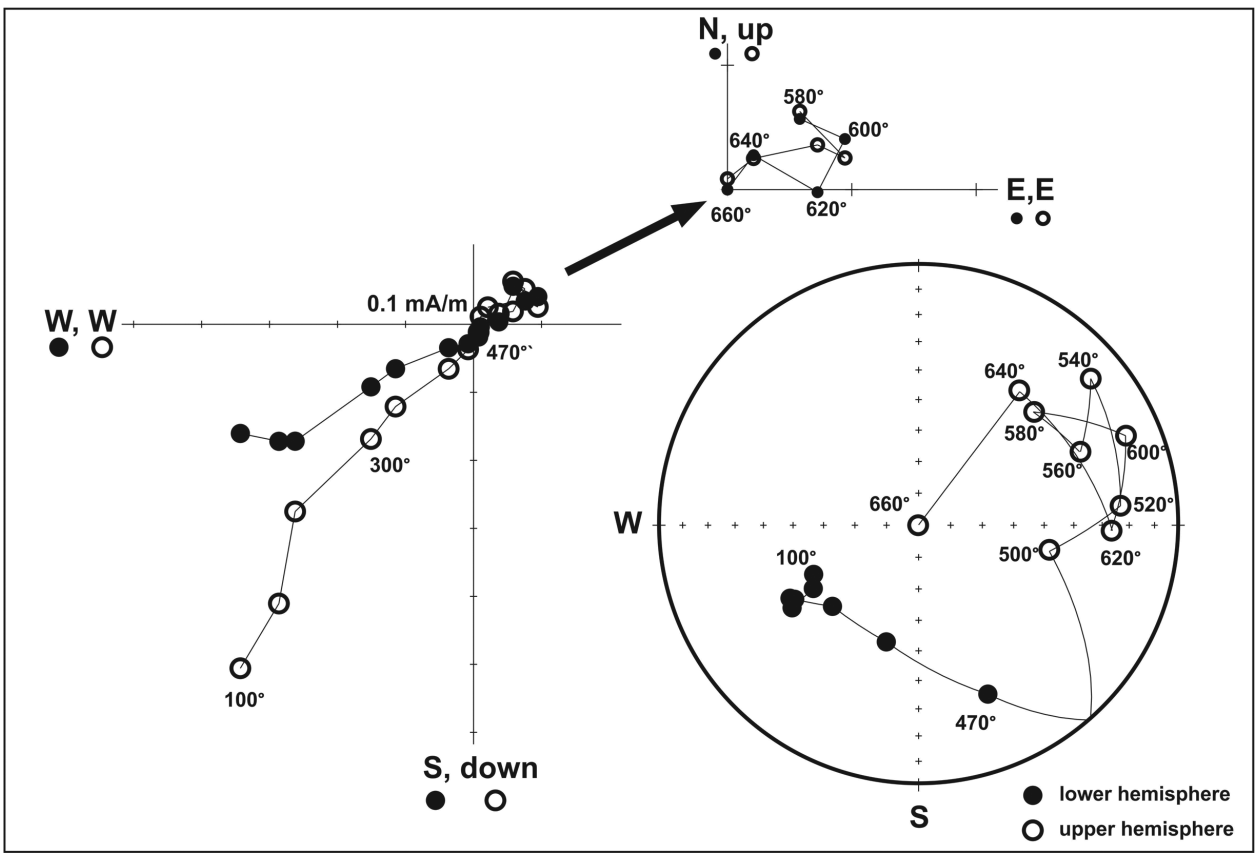

Figure 9. Thermal demagnetization results (vector component diagram and stereogram) of a representative early Silurian sample with high-temperature reversed polarity component. A detailed view of the last four heating steps is shown at the top. Stratigraphic coordinates are used.

Table 4. A compilation of palaeomagnetic data from the south of the Siberian platform, interpreted by us to be the result of a regional remagnetization. Coordinate system indexes: I, *in situ*; N, recalculated to coordinates of Nyuya River mouth; V, same, corrected for Vilyuy rifting by rotating the poles from the Angara Block 20° CW around an Euler pole of 62°N 117°E. (Pavlov *et al.* 2008).

	Object, geography	Coordinate system	D	I	K	Alfa95	Plat (°)	Plong (°)	A95(°); dp/dm (°)	Reference	Comments
1	MT component in Late Ordovician and Early Silurian sedimentary rocks. Nyuya Rv. mouth λ=116.3° E, φ=60.7° N.	I, N	204.4	37.9	27.2	2.7	-5.9	93.2	2.5; 1.9/3.2	This study	Pre-folding magnetization
2*	Late Riphean mafic sills (sills 4+7+8). Prilenskaya fold-and-thrust zone and Urinski anticlinorium; λ=117.2°E;φ=60.0°N	I	19.7	-52.3	217.4	8.4	4.3	100.7	9.6; 7.9/11.5	[Shatsillo et al. 2004]	After-folding magnetization; pole calculated for normal-polarity direction
		N	198.5	51.7							
3*	Late Riphean mafic sills (sills 5+6+9). Prilenskaya fold-and-thrust zone and Urinski anticlinorium; λ=117.2°E;φ=60.0°N	I	23.5	-49.7	15.3	32.6	2.6	97.1	35.4; 28.9/43.4	[Shatsillo et al. 2004]	Syn-folding magnetization; pole calculated for normal-polarity direction
		N	202.3	49.2							
4	Vendian Tirbesskaya formation.Prilenskaya fold-and-thrust zone and Urinski anticlinorium. λ=117.5°E; φ=60.0°N;	I	200.6	55.6	71.9	4.7	7.6	100.8	5.7; 4.8/6.7	[Shatsillo et al. 2004]	
		N	199	55.1							
5**	Polovinka village; λ=113.7° E, φ=60.1 N		177	25.4	18.2	3.6	-16.5	116.7	2.8; 2.1/3.9	[Pavlov et al., 1999]	
		N	179.6	24.4							
6	Polovinka village. λ=113.7° E, φ=60.1°N	I	188.1	37.6	11	5.7	-8.6	106.1	5.2; 4.0/6.7	This study	Reinterpretation of #5. We have used unambigous secondary components only
		N	190.8	36.4							
7	Village Krivaya Luka, λ=107.8°E; φ=57.6°N.	I	176.5	30	32	3.9	-16.2	111.3	3.2; 2.4/4.3	[Rodionov et al., 2003]	
		N	184.9	24.8							
8***	Nyuya syncline λ=116.3°E, φ=60.7°N. Early Silurian sedimentary rocks	N	195.8	43.4			-3	102	8.9	[Rodionov et al., 1982]	
9	Vicinity of Kudrino Village. λ=108.0° E, φ=57.7°N	I	185.7	20.2	16.2	13.2	-21.7	102	10; 7.2/13.8	[Pavlov et al., 2008]	
		N	193.4	13.4							
		V	213.4	13.2							
10	B. Zhidoi R. Early Vendian. λ=103.0°E;φ=52.0°N. Jid-2 component	I	174.3	44.2	177.4	4.5	-11.9	113.2	4.5; 3.5/5.6	[Shatsillo 2005]	Declination and inlination in geographic coordinates; pole calculated for normal-polarity direction
		N	183.2	32							
		V	208.4	31.6							
11	Midde Angara river, Middle-Late Ordovician, λ=99.8°E;φ=58.5°N. Tilt corrected		188.1	39.6	6.9	15.2	-8.7	92.2	14.1	[Pavlov et al. 2012]	
		N	205.1	33.1							
		V	225.2	32.8							

*These directions were characterized by reversed magnetic polarity, and have been inverted to normal polarity.
**Pavlov *et al.* (1999) isolated a secondary intermediate component in the middle Ordovician sedimentary section near Polovinka Village on the Lena River. It has been subsequently shown in Shatsillo *et al.* (2004), that this component can sometimes fully overprint the primary HT component of middle-Ordovician age. Thus, it is possible to mistake the secondary MT component for the primary HT component, and vice versa. To avoid this problem, we have recalculated the data set from Pavlov *et al.* (1999) using only those samples in which this component is clearly interpreted as intermediate and can be isolated unambiguously.
***The palaeomagnetic direction recorded in Silurian rocks of the Nyuya syncline was initially interpreted by Rodionov *et al.* (1982) as a primary NRM component. We reinterpret that direction as either heavily contaminated by the intermediate component or as solely MT. The thermal cleaning method used in Rodionov *et al.* (1982) was limited to a single heating step of 400 °C. As shown by our data, the MT components in Silurian rocks of the Nyuya syncline are often characterized by higher unblocking temperatures, which would not be erased by a 400 °C heating step.

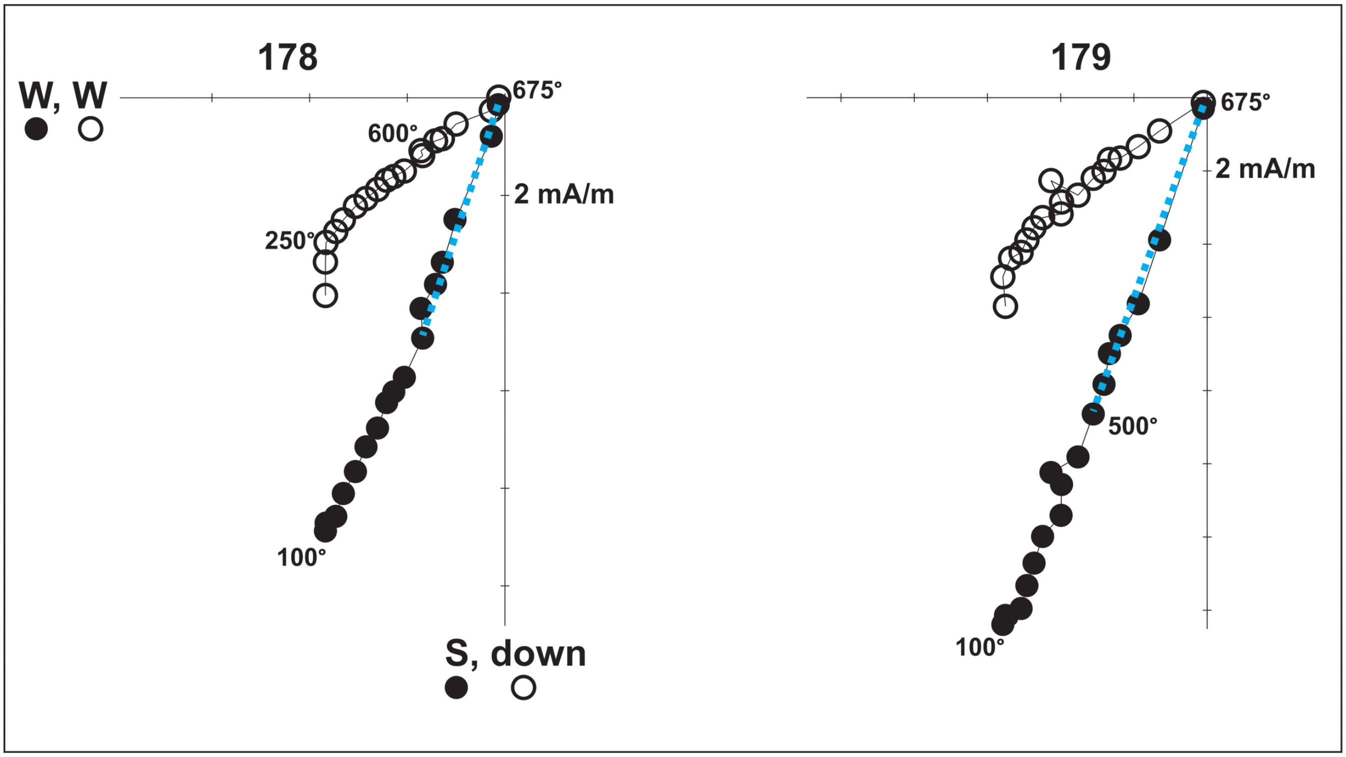

Figure 10. Thermal demagnetization results of representative late Silurian (Neryukteiskaya formation) samples bearing high-temperature component (HT_{s_ner}). Stratigraphic coordinates are used.

highest among all samples: they vary from 6×10^{-3} to 2×10^{-2} A m^{-1}. We were able to isolate a high-temperature component in all 23 samples, and $HT_{s(ner)}$ always decayed towards the origin on orthogonal diagrams. The unblocking temperatures were invariably located near the Curie temperature of haematite.

The average direction of $HT_{s(ner)}$ did not differ statistically from the average direction of the Melichanskaya and Utakanskaya formations (Table 3). Thus, we have calculated an all-Silurian average direction using Melichanskaya + Utakanskaya (54 samples) and Neryukteiskaya (23 samples) formations. The resulting direction successfully passed the DC fold test. This direction was used to calculate a palaeomagnetic pole #14 in Table 5.

Mean palaeomagnetic directions and palaeomagnetic poles

We have isolated three stable magnetization directions: HT_o, HT_s and MT (Table 2 and Fig. 12), whose directions are statistically different at 95 per cent confidence level (Table 3). Palaeomagnetic poles calculated for these components, according to Fisher (1953), are shown in Table 2.

GEOCHRONOLOGICAL RESULTS

Sample VP-VI-Le-1

Nine zircons were analysed. The plot of $^{206}Pb/^{238}U$ ages (Fig. 13) shows some dispersion consistent with a small amount of inheritance. The crystallization age of this rock is obtained by a cluster of the three youngest which have a weighted mean $^{206}Pb/^{238}U$ date of 377.72 Ma ± 0.12/0.25/0.48 (2σ, mean square weighted deviation (MSWD) = 0.40). U-Th-Pb data for each spot analysis are presented in Table B1 (Appendix B).

Sample VP-VII-Mu-1

The crystallization age of this rock is obtained from the ^{204}Pb-corrected $^{238}U/^{206}Pb$ ages of the six oldest grains (Fig. 14) with the weighted mean of 371.0 ± 3.3 Ma (95 per cent confidence, MSWD = 4.1). Two analyses (spots 1.1 and 8.1), which were not included in calculations, have slightly younger ages probably due to lead loss. We interpret the 371.0 ± 3.3 Ma age as the crystallization age for the mafic sill. U-Th-Pb data for each spot analysis are presented in Table B2 (Appendix B).

DISCUSSION

Age of components

The palaeomagnetic data can be used to constrain the palaeogeographic positions of the Siberian platform during middle Palaeozoic. However, it is essential to estimate the age of the isolated palaeomagnetic components before interpreting palaeomagnetic components in terms of palaeogeographic positions.

The depositional ages of the sediments are, obviously, the oldest limits for magnetization. The isolated average components—HT_o, HT_s and MT—successfully pass fold test (Table 2), thus are pre-folding. Therefore, the age of folding is the younger limit for magnetization. We obtained the older constraint for the folding by dating the two folded sills. The youngest sill yielded a 371.0 ± 3.3 Ma age, which corresponds to the Famennian age. Therefore, the folding must have happened during or after the Famennian age of late Devonian. The 310–270 Ma post-orogenic granites of the Angara–Vitim batholith truncated the strata and fold-and-thrust deformations in the Patom Belt to the south of the study area. Thus, these granites probably signify the youngest constraint for the Patom folding. To summarize, the folding must have taken place

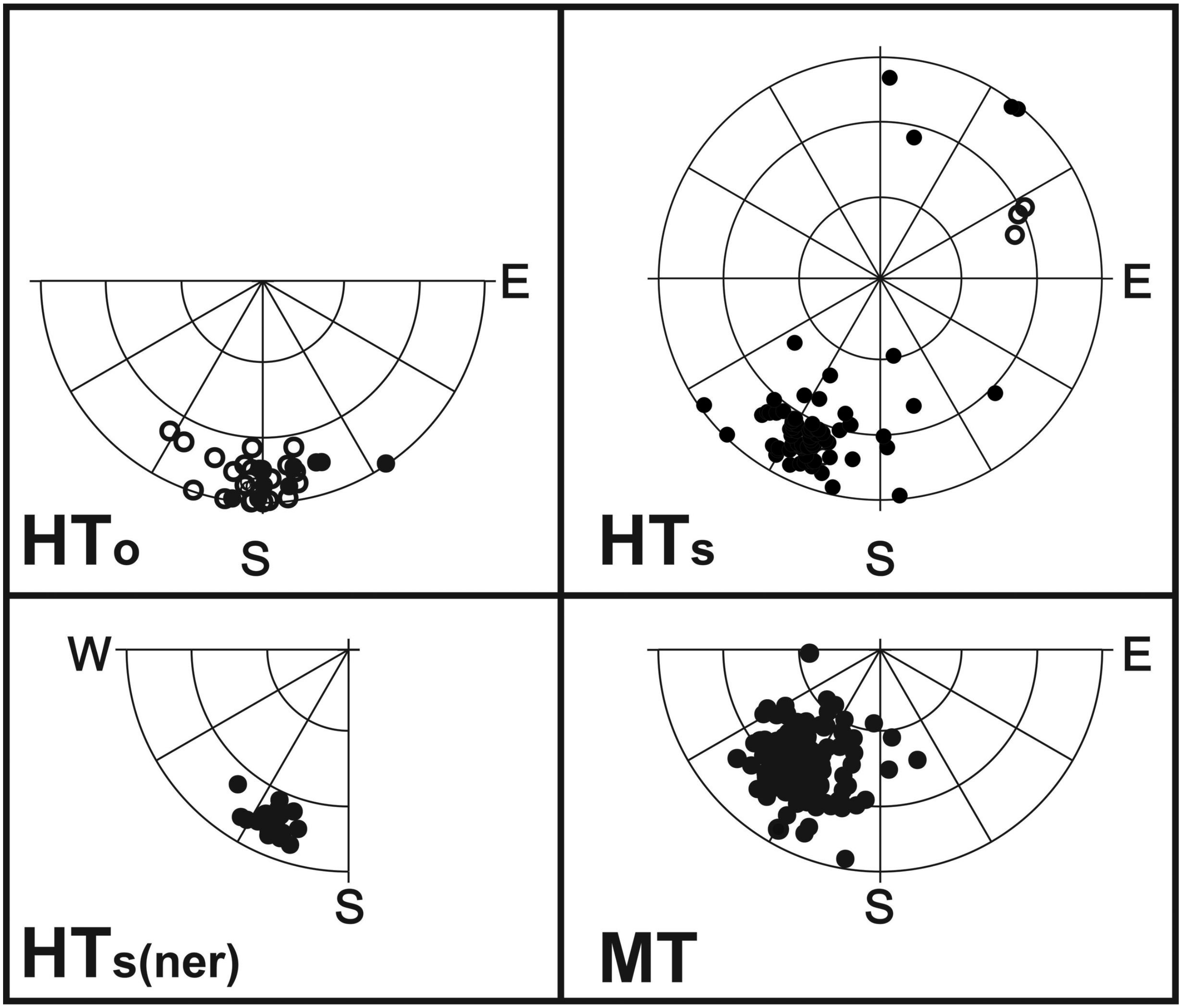

Figure 11. Equal-area projection showing the distribution of characteristic and less stable components. Open/filled circles represent projections on upper/lower hemisphere, respectively. Stratigraphic coordinates are used.

after 371.0 ± 3.3 Ma and less confidently, ended prior to 310 Ma. The important episodes of sedimentation, magnetization, magmatism and tectonics that constrain the age of folding are shown in Fig. 15.

HT components in Ordovician and Silurian samples can be considered primary, that is, equal in age, or negligibly younger, than the time of sedimentation, based on the following arguments: (1) fold tests yield positive results; (2) in the case of the HT_s component, both polarities are present; (3) calculated poles do not coincide with any of the known younger Siberian poles. The two HT components, HT_s and HT_o, are statistically different from each other and from the MT component (Table 4).Therefore, we assign late Ordovician and early Silurian ages for the corresponding directions.

The average directions of the two MT components, MT_o and MT_s, do not differ statistically at the 95 per cent confidence level (Table 4), making it permissible and reasonable to join them. The combined MT component is secondary, since it is found in rocks of different ages. We have shown that MT post-dates the early Silurian sedimentation and pre-dates the post-late Devonian folding, but its age can be further confined because its palaeomagnetic pole is located in the 'older' part of the Siberian apparent polar wander (APW) trend (e.g. Smethurst *et al.* 1998; Cocks & Torsvik 2007) relative to the late Devonian and Carboniferous poles reported by Shatsillo *et al.* (2013) and Kravchinsky *et al.* (2002) (age refined in Courtillot *et al.* 2010), respectively. This puts MT in the time frame between late Silurian and late Devonian.

In addition, the MT component is in a good agreement with late Silurian–early Devonian palaeomagnetic data reported for the Tuva terrain, which by Silurian had already accreted to the Siberian platform (Didenko *et al.* 1994). The mean palaeomagnetic inclination of 42.1° obtained from late Silurian–early Devonian sediments of the Tuva terrane (Bachtadse *et al.* 2000) indicated lower palaeolatitudes for the Siberian continent compared to those previously published. Due to the dispersion of magnetic declinations in the Tuva samples, probably caused by vertical-axis block rotations, it is

Table 5. A compilation of middle Ordovician–Devonian palaeomagnetic data for Siberian platform. *N*, number of samples; long and lat, longitude and latitude of sampled location; Plat and Plon, latitude and longitude of palaeomagnetic pole; α95 and d*p*/d*m*: statistical 95 per cent confidence parameters; block, An: Angara, Al: Aldan blocks of Siberian platform. 'corr.' designates poles corrected for Vilyuy rifting (see text).

	Object	Age of magneti-zation	*N*	long	lat	Plat	Plon	α95 or d*p*/d*m*	Block	Reference
1	Moyero rv.	O2lla	32	104	67.5	−22.7	157.6	2.0/3.8	An	(Gallet & Pavlov 1996)
2	Kulyumbe rv.	O2lla	14	88.8	68	−24.1	152.4	2.4/4.5	An	(Pavlov *et al.* 2008)
3	Polovinka section, Lena rv. (K1 component)	O2lla	80	113.7	60.1	−31.2	133.2	2.3/4.6	Ald	(Pavlov *et al.* 1999)
3corr.						−26.9	155.5	2.3/4.6	An	
4	Lena rv.	O2lla		118.1	59.8	−32	139.4	1.6/3.1	Ald	(Torsvik *et al.* 1995)
4corr						−26.8	161.5	1.6/3.1	An	
5	Kudrino section	O2lla		108	57.7	−21.1	143.4	2.7/5.3	Ald/An	(Pavlov *et al.* 2008)
6	Stolbovaya rv.	O2lla	2 end-points + 30 great circles	92.5	62.1	−22	158	2.9/5.5	An	
7	Rozhkov section, Angara rv.	O3car	24	100	58.8	−29.5	140.2	4.5/9.0	An	(Pavlov *et al.* 2012)
8	Nyuya rv. (HT$_o$)	O3car-ash	9 sites, 38 samples	116.3	60.6	−31.3	129.5	2.6/5.1	Ald	This study
8corr.						−27.5	152.0		An	
9	Lena rv.	O2lla	26			−32	139	1.6/3.1	Ald	(Torsvik *et al.* 1995)
9corr.						−26.9	161.1	1.6/3.1	An	
10	Lena rv.	O3ash	17			−21	109	9.2/17.8	Ald	
10corr.						−20.6	130.3	9.2/17.8	An	
11	Lena rv.	O3ash-Sil	9	116.4	60.5	3	118.1	13.1	Ald	
11corr.						4.6	135.2	14.8	An	
12	Moyero rv.	O3ash-S1	20	104	67.5	−13.9	124.1	4.2/8.3	An	(Gallet & Pavlov 1996)
13	Lena rv.	S1		116	60.3	−3	102	8.9	Ald	(Rodionov *et al.* 1982)
13corr.						−4	120.3	8.9	An	
14	Nyuya and Lena rv. (HT$_S$)	S1-S2lud	77	116.3	60.6	−17.6	102.0	2.3/4.4	Ald	This study
14corr.						−18.4	122.7	2.3/4.4	An	
15	Nyuya and Lena rv. (MT)	S2-D1?	104 samples	116.3	60.6	−5.9	93.2	1.9/3.2	Ald	
						−8.2	112.0		An	
16	Nyuya and Lena rv. (HT$_S$)	S1-S2lud	56	116.3	60.6	−18.6	101.9	4.6	Ald	(Shatsillo *et al.* 2007)
17	Nyuya and Lena rv. (MT$_S$)	S2-D1?	39	116.3	60.6	2.6	97.9	5.6	Ald	
18	Tuva (Elegest 1 + 2)	S2-D1	187	93.8	51.2	−26.3	144	4.3	An	(Bachtadse *et al.* 2000)
19	Tuva (Kadvoy)	S2-D1	30	93.8	51.2	−13.3	63.7	6.4	An	
20	Tuva (Chadan)	S2-D1	37	91.7	51.3	−11.9	113.2	8.3	An	

Table 5 (*Continued.*)

	Object	Age of magneti-zation	*N*	long	lat	Plat	Plon	α95 or d*p*/d*m*	Block	Reference
21	Tuva (Us1)	S2	10	92.9	52.2	−10.1	113.3	8	An	
22	Tuva (Us2)	S2	5	92.9	52.2	−3	142.2	15.6	An	
23	Tuva (Us3)	S2	9	92.8	52.1	−13.7	80.4	6.7	An	
24	Vilyuj and Markha rv.	D3		116	63.5	11.1	149.7	8.9	n/a	(Kravchinsky *et al.* 2002), age of rocks refined in (Courtillot *et al.* 2010)

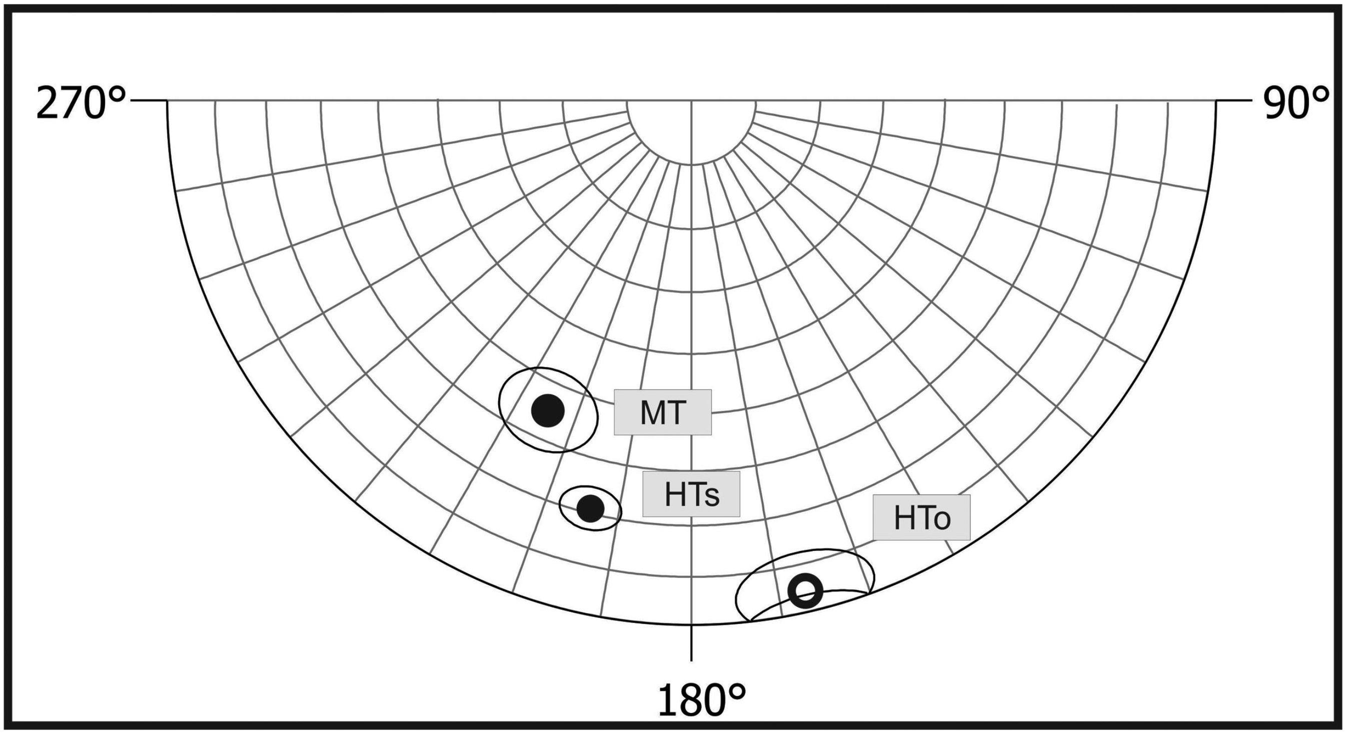

Figure 12. Equal-area projection of the mean directions of isolated components. Open/filled circles represent projections on upper/lower hemisphere, respectively. Outer circles represent 95 per cent confidence intervals. Stratigraphic coordinates are used.

not possible to compare the palaeomagnetic poles from the Siberian platform and the Tuva terrane directly. Instead, we have recalculated palaeomagnetic directions from this study, corrected for Vilyuy rifting as suggested in Pavlov *et al.* (2008), into Tuva coordinates. The resulting inclinations for HT_s and MT components are 28.9° and 44.9°, correspondingly. The inclination of MT component is statistically indistinguishable from the late Silurian–early Devonian mean Tuva inclination ($\gamma/\gamma_{cr} = 2.8 \pm 8.3°$), suggesting that the formation of the MT component may have taken place close to the Silurian–Devonian boundary, most probably in early Devonian.

Similar intermediate components were reported for the rocks of different ages along the southern margin of Siberian platform, well outside of Nyuya syncline. We have summarized such data, including the MT component from this study (Table 4 and Fig. 16). The studied rocks vary in age from Neoproterozoic (directions #2, 3 in Table 4) to early Silurian (directions #1, 8). Geographically, the sampling locations are separated by up to 1200 km. We can assume that the intermediate secondary components in Silurian and Ordovician rocks were caused by a regional-scale remagnetization event that influenced the southern margins of Siberian platform in post-Silurian time.

Choice of polarity

Choosing the correct polarity is a decision of utmost importance, since it defines the hemisphere of a crustal block on Earth's surface. The opposite polarity interpretation will rotate the block 180° around the vertical axis, and place it in the opposite hemisphere at an equal distance from the equator. In extreme situations with steep palaeomagnetic inclinations, the wrong choice of polarity interpretation could result in an error of up to one-half of Earth's circumference.

The polarity selection in this study—normal for most of the samples, reversed for some—was based on the principle of minimizing the required displacements and rotations of the Siberian platform and on comparison with the sequence of younger palaeomagnetic poles for the Siberian platform:

(1) Contemporary palaeomagnetic poles for any continent, averaged over sufficient time to eliminate the effect of secular variations, coincide with the geographical north pole.

(2) Mesozoic palaeomagnetic poles for the Siberian continent are located in the Arctic Ocean (Pavlov 2012).

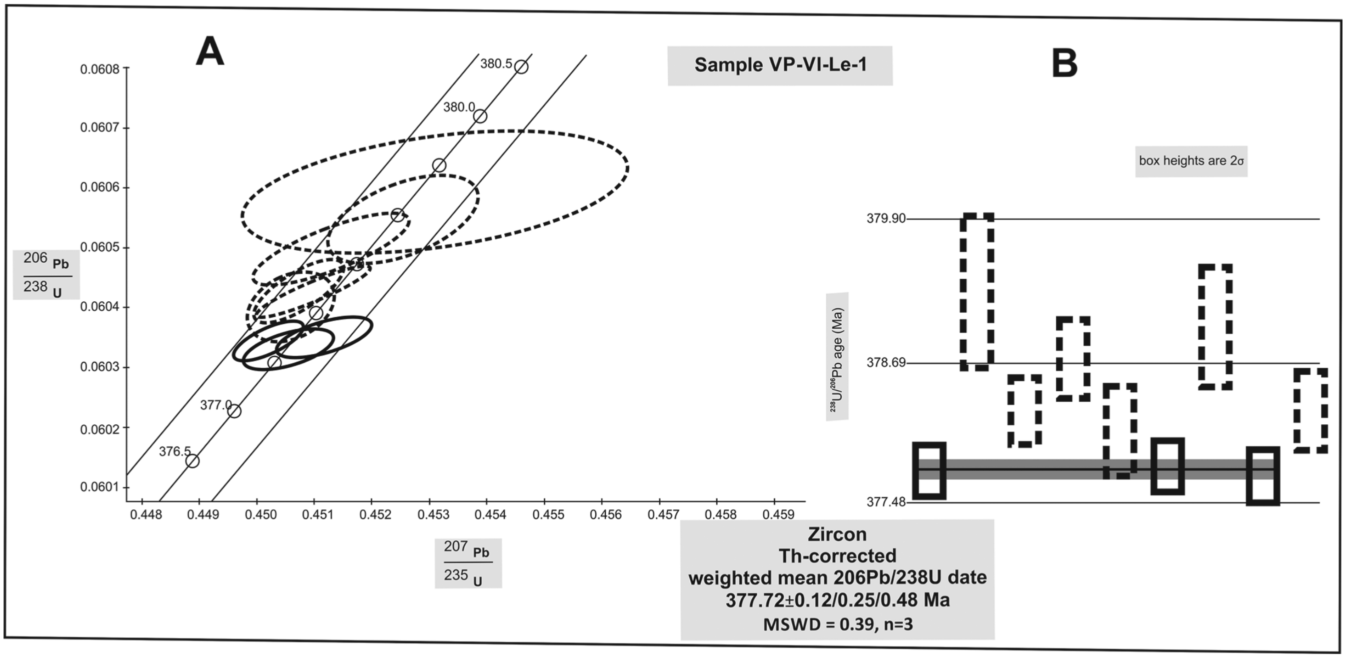

Figure 13. Results of U-Pb dating of the sill (sample VP-VI-Le-1). (a) Concordia diagram. (b) a plot of weighted average $^{206}Pb/^{238}U$ ages. Grey rectangle represents the mean age with embedded uncertainties.

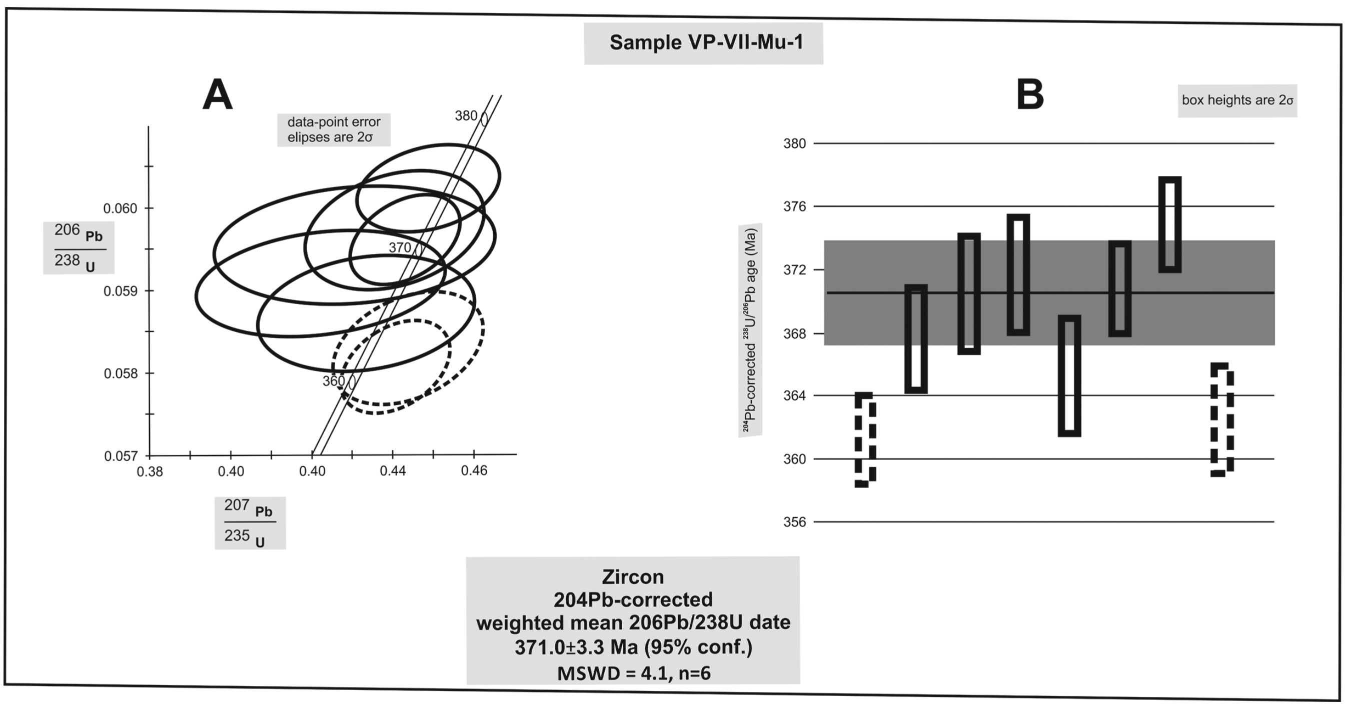

Figure 14. Results of U-Pb dating of the sill (sample VP-VII-Mu-1). (a) Concordia diagram for sample VP-VII-Mu-1. (b) A weighted average plot of $^{206}Pb/^{238}U$ ages.

(3) The Permo-Triassic Siberian palaeomagnetic north pole acquired from the Siberian Traps is located along the western coast of Kamchatka Peninsula (Pavlov *et al.* 2007).

(4) The pole that we have acquired from ∼300 Ma igneous rocks of the Angara–Vitim batholith was used as a benchmark (Shatsillo *et al.* 2013). These post-tectonic granites intruded the southern margin of the Siberian platform during the Permian–Carboniferous long interval of reversed polarity—the Kiaman Superchron (Khramov 1958, 1967; Irving & Parry 1963; Eide & Torsvik 1996). The palaeomagnetic north pole of the batholith (Plon = 126.2; Plat = 38.3) is located in east Asia.

(5) The *ca.* 374 Ma pole by Kravchinsky *et al.* (2002), which was initially assigned a late Devonian–early Carboniferous age and was later corrected by Courtillot *et al.* (2010), is situated in the Pacific Ocean to the east of Eurasia.

Therefore, as noted much earlier by Khramov (1974), there is an obvious northward migration of palaeomagnetic poles for the

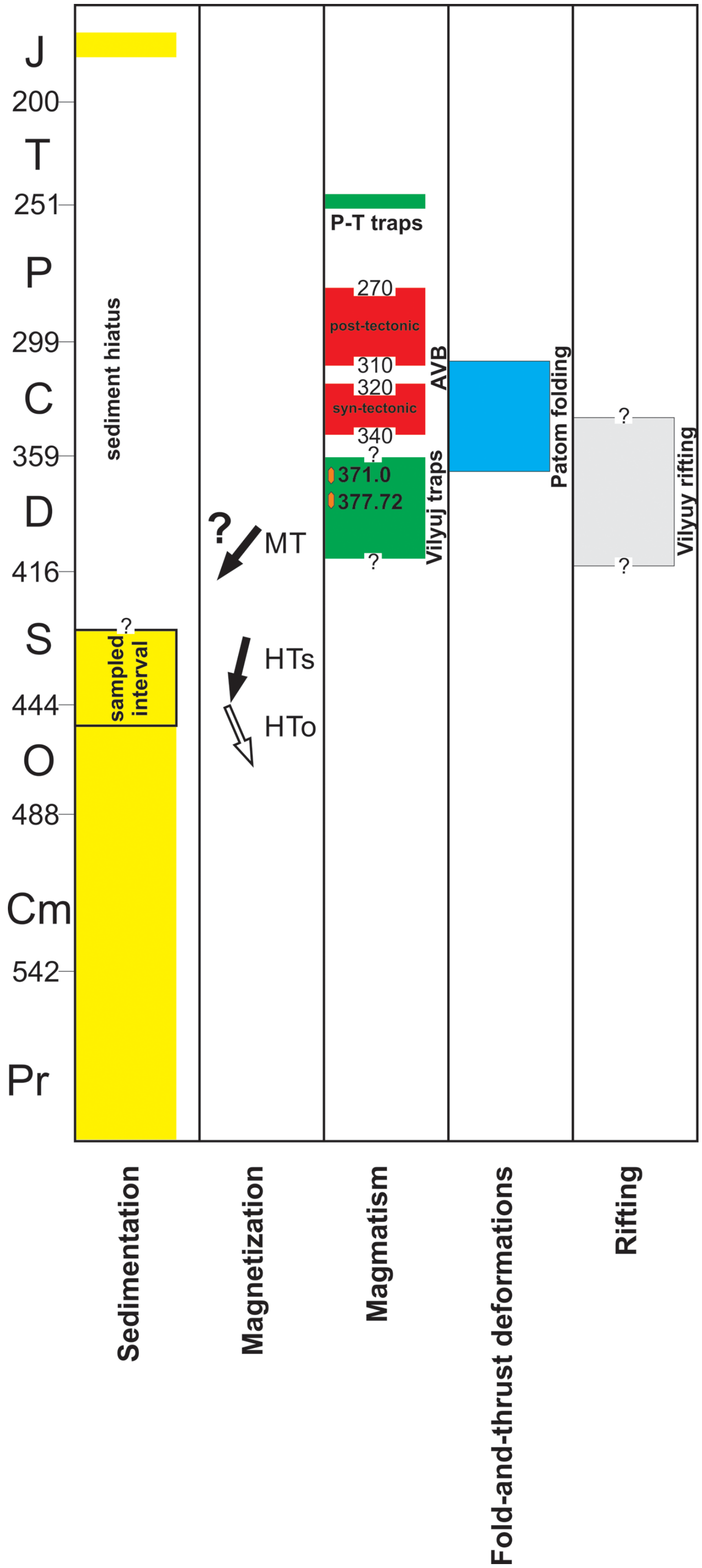

Figure 15. Schematic representation of key episodes of sedimentation (yellow), igneous activity (red: felsic, green: mafic), rifting (grey), and folding deformations (blue) in the vicinity of the Nyuya syncline and in the Baikal–Patom fold-and-thrust belt. The new geochronology data from the mafic sills constrains the folding. Timing for AVB emplacement is taken from Tsygankov *et al.* (2007).

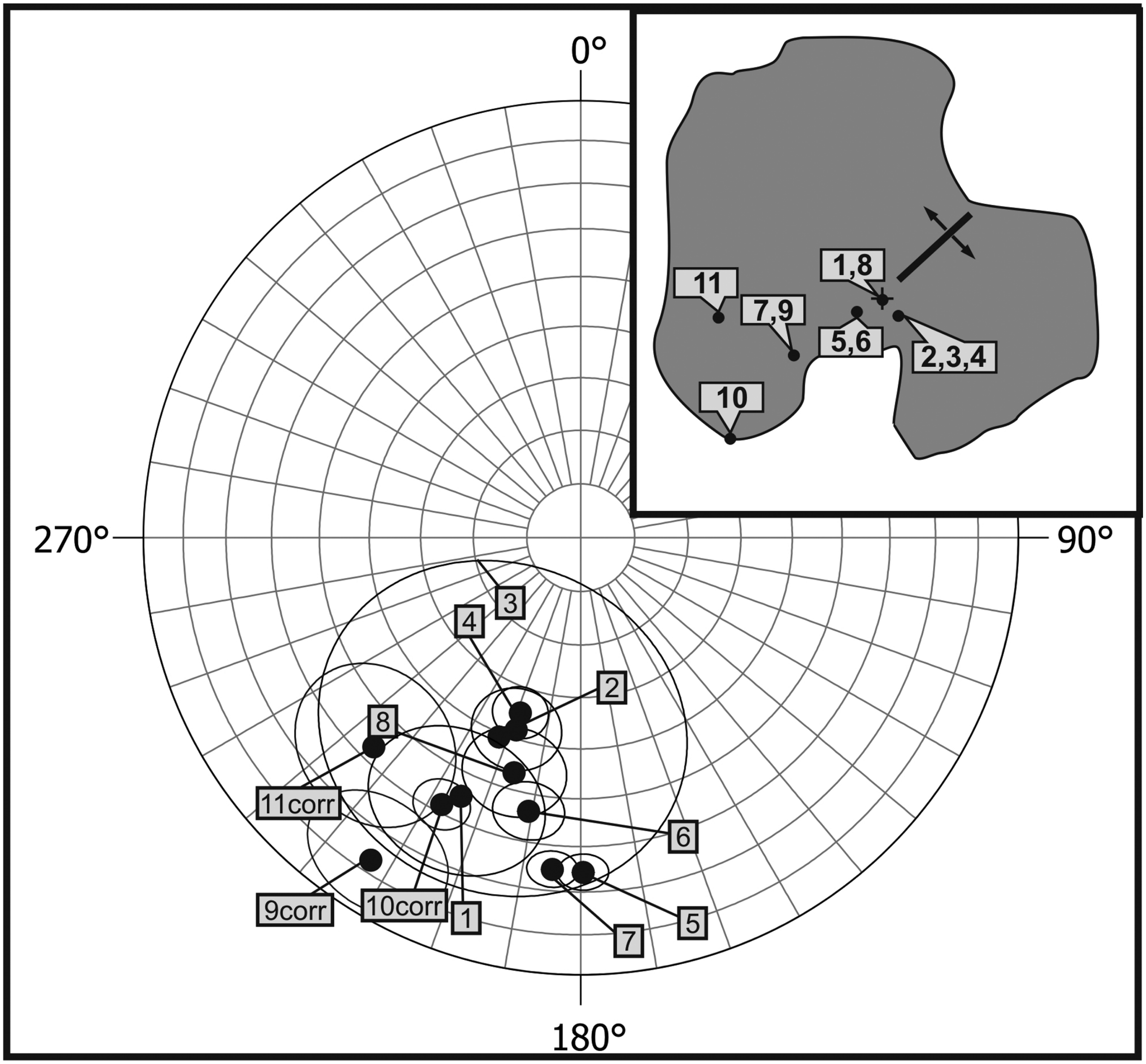

Figure 16. Equal-area projection of the remagnetization directions. Inner circles indicate directions; outer circles represent uncertainty intervals. Labels correspond to Table 4. All directions have been recalculated into Nyuya River mouth coordinates ($\lambda = 116.3°$E, $\varphi = 60.7°$N). Directions ##9–11 were acquired from the Aldan Block. Here they are rotated into the reference frame of the Angara Block to correct for Vilyuy rifting (see text). Inset: simplified sketch of the Siberian platform with sampling locations. Approximate location of the Vilyuy palaeorift is shown as a solid line with arrows.

Siberian platform in the Phanerozoic. This migration fits well with our choice of polarity option. Flipping the polarity interpretation (and hence the hemisphere) for Ordovician–Silurian rocks would require an unusually fast N–S drift episode, and a rapid rotation of the platform about a vertical axis. We have chosen to stay on the conservative side by minimizing the required displacements and rotations.

Comparison of calculated poles with published palaeomagnetic data

Data, presented in Pavlov *et al.* (2008) indicated that during the middle-late Palaeozoic the Aldan and Angara–Anabar blocks, composing the Siberian platform, had experienced relative rotation (Fig. 17) in a major Vilyuy rifting event (Masaitis *et al.* 1975). Our study area is entirely located on the Aldan Block (Fig. 17), to which we apply a tectonic rotation of 20° counter-clockwise (CCW) around an Euler pole at 62°N 117°E, as suggested in Pavlov *et al.* (2008). By doing this, we have rotated the data from the Aldan Block into the Angara reference frame, correcting for the Vilyuy rifting. The newly acquired poles are reported in both reference frames (Table 5), and the corrected poles are denoted by an index ‘corr’.

The calculated late Ordovician pole is situated near the southern coast of modern Australia (Fig. 18). Our early Silurian pole lies to the northwest, in the Indian Ocean. The palaeomagnetic

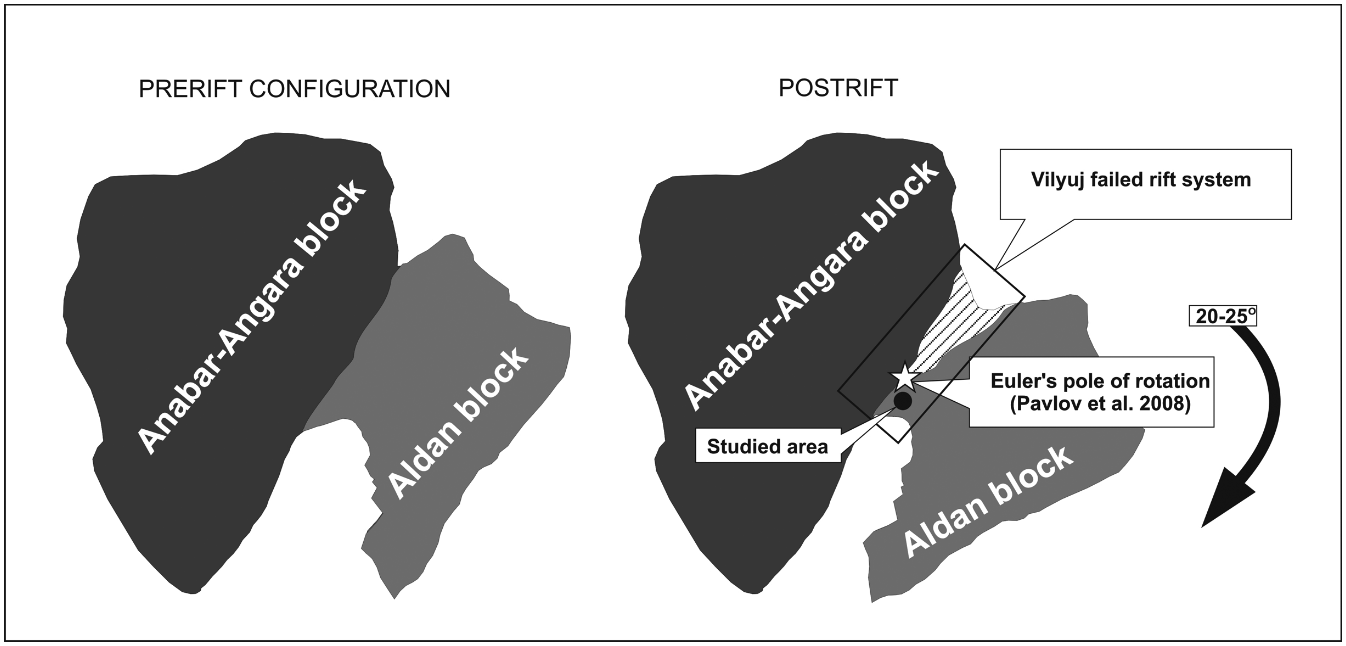

Figure 17. Configuration of the Siberian platform before (a) and after (b) the Devonian–Carboniferous Vilyuy rifting.

pole derived from the early Devonian (?) MT component is also located in the Indian Ocean, although closer to the equator.

Our late Ordovician pole is located near the cluster of middle Ordovician poles ##1, 3, 4, 5 (the numerals here and later correspond to Table 5) reported for both the Aldan (Fig. 18) and Angara (Fig. 19) blocks. This suggests that there was little or no rotation and latitudinal drift of the Siberian platform from middle to late Ordovician time. Some of the published late Ordovician poles (##7, 10) are located in between our late Ordovician and early Silurian poles within their reliability intervals, indicating the migration path of the poles. Pole #11 is an obvious outlier (Fig. 18) and is probably the result of the regional remagnetization. We reinterpret the early Silurian pole #13, acquired by Rodionov *et al.* (1982) from our study section, as either heavily contaminated by an intermediate component or as solely MT. The thermal cleaning method used in Rodionov *et al.* (1982) was limited to a single heating step of 400 °C, whereas our data show that intermediate components in Ordovician–Silurian sediments are often characterized by higher unblocking temperatures.

An early Silurian pole #16, derived by us earlier from a smaller set of samples (Shatsillo *et al.* 2007) is indistinguishable 95 per cent confidence from the newly acquired Silurian pole. The pole of remagnetization derived from the MT component, however, is notably different. The intermediate component in Silurian rocks, presented in Shatsillo *et al.* (2007) resulted in a pole #17 located near the west coast of Malaysia (Fig. 18). Increasing the number of results for the Silurian interval by adding data from the Ordovician sediments shifted the resulting pole of remagnetization 12° to the SSW.

Discussion regarding the possibility of inclination shallowing

While many sedimentary rocks are able to record the true direction of the geomagnetic field, there are also numerous examples when recorded inclination (and, therefore, the final palaeomagnetic result) can be seriously affected by compaction-induced and/or (less frequently) syn-sedimentary inclination shallowing. Several experimental and numerical techniques to detect and correct this inclination bias have been developed in recent years (Tan & Kodama 2003; Tauxe & Kent 2004). Unfortunately, the number of collected samples and the amount of sample material currently at our disposal are not sufficient to implement these techniques. Nevertheless, we can suggest two arguments which seemingly indicate that obtained results have not been appreciably affected by inclination flattening. The first one is that carbonate or carbonate-rich sedimentary rocks (like the ones considered in this study) experience cementation at the earliest stages of their diagenesis, soon after sedimentation, and therefore are not heavily affected by inclination shallowing compared to clastic rocks. The second and, we believe, an even stronger argument comes from comparison of nearly coeval poles from widely separated regions of the Siberian platform and its margins. Inclination shallowing shifts the calculated palaeomagnetic pole farther from the sampling locality along the great circle passing through the sampling locality and the 'true' palaeomagnetic pole. Our data do not exhibit such a far-sided effect. On the contrary, the late Ordovician–early Silurian pole from Moyero River (#12 in Table 5) is statistically indistinguishable ($4.0 \pm 5.0°$; Debiche & Watson 1995) from our Silurian S_1 pole after applying the correction for Viluy rifting (Fig. 19). Moreover, the angular difference between the two poles becomes even less ($3.4 \pm 5.7°$) when late Silurian data are omitted and only early Silurian samples are used. The late Ordovician poles from the Rozhkov section (#7 in Table 5) and Nyuya section (O_3), though close, are statistically different, but neither is significantly farther from the sampling site than the other (Fig. 19). Finally, an almost perfect agreement of our late Silurian–early Devonian palaeomagnetic direction, recalculated into Tuva coordinates, with coeval direction from Tuva region (see discussion above) further supports the absence of considerable inclination shallowing in Lena–Nyuya rocks. Note as well that the secondary late Silurian–early Devonian magnetization had formed long after sedimentation; therefore it too should be immune to inclination flattening.

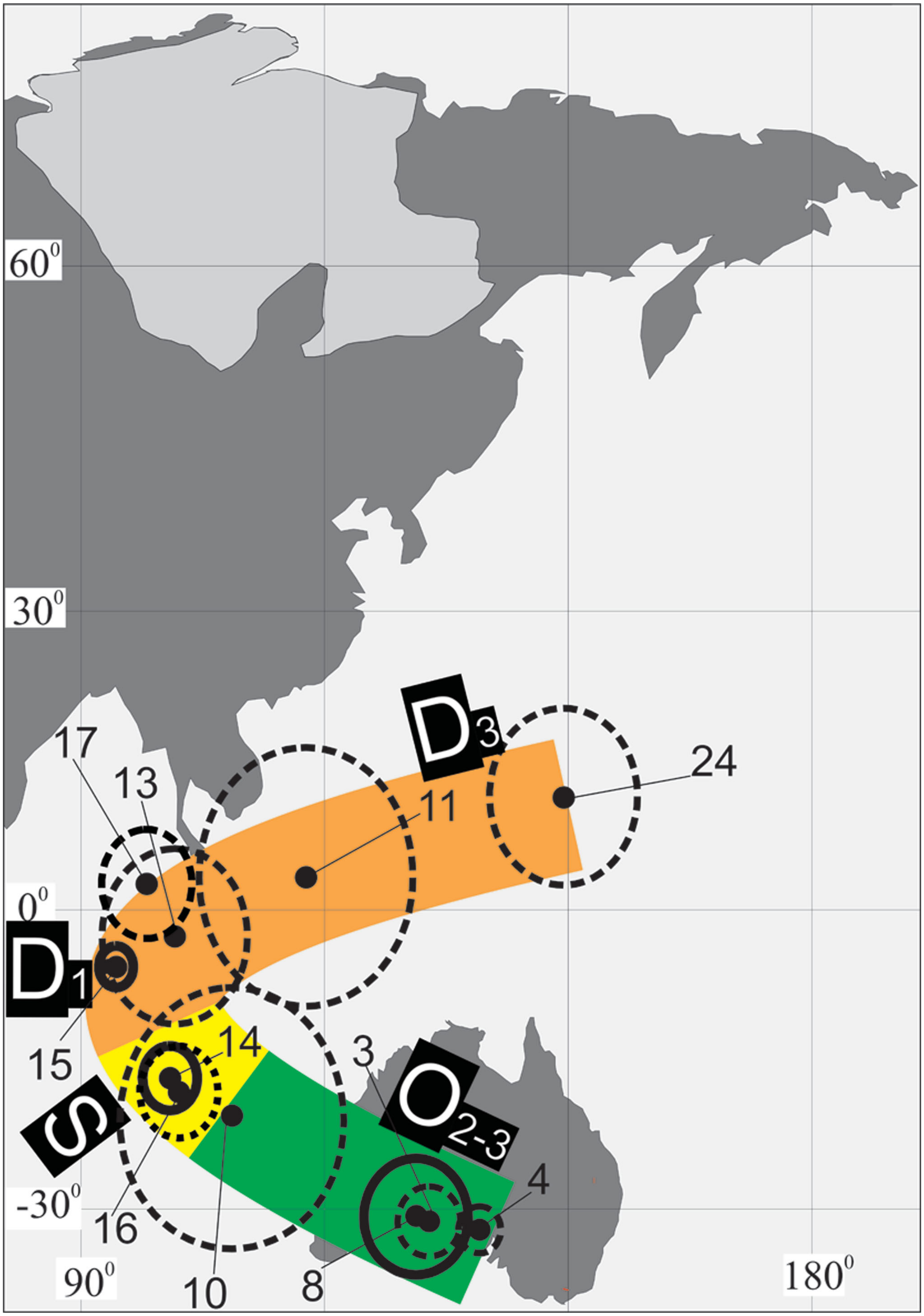

Figure 18. Palaeomagnetic poles from the Aldan Block of Siberia for middle Ordovician–early Carboniferous. Inner circles give the locations of the poles and the outer circles represent 95 per cent confidence areas (solid lines for the poles from this study and dashed lines for literature poles). We have also included the D_3 pole by Kravchinsky *et al.* (2002). This pole probably post-dates Vilyuy rifting. Therefore, it is shown in its own coordinates, not corrected for Vilyuy rifting.

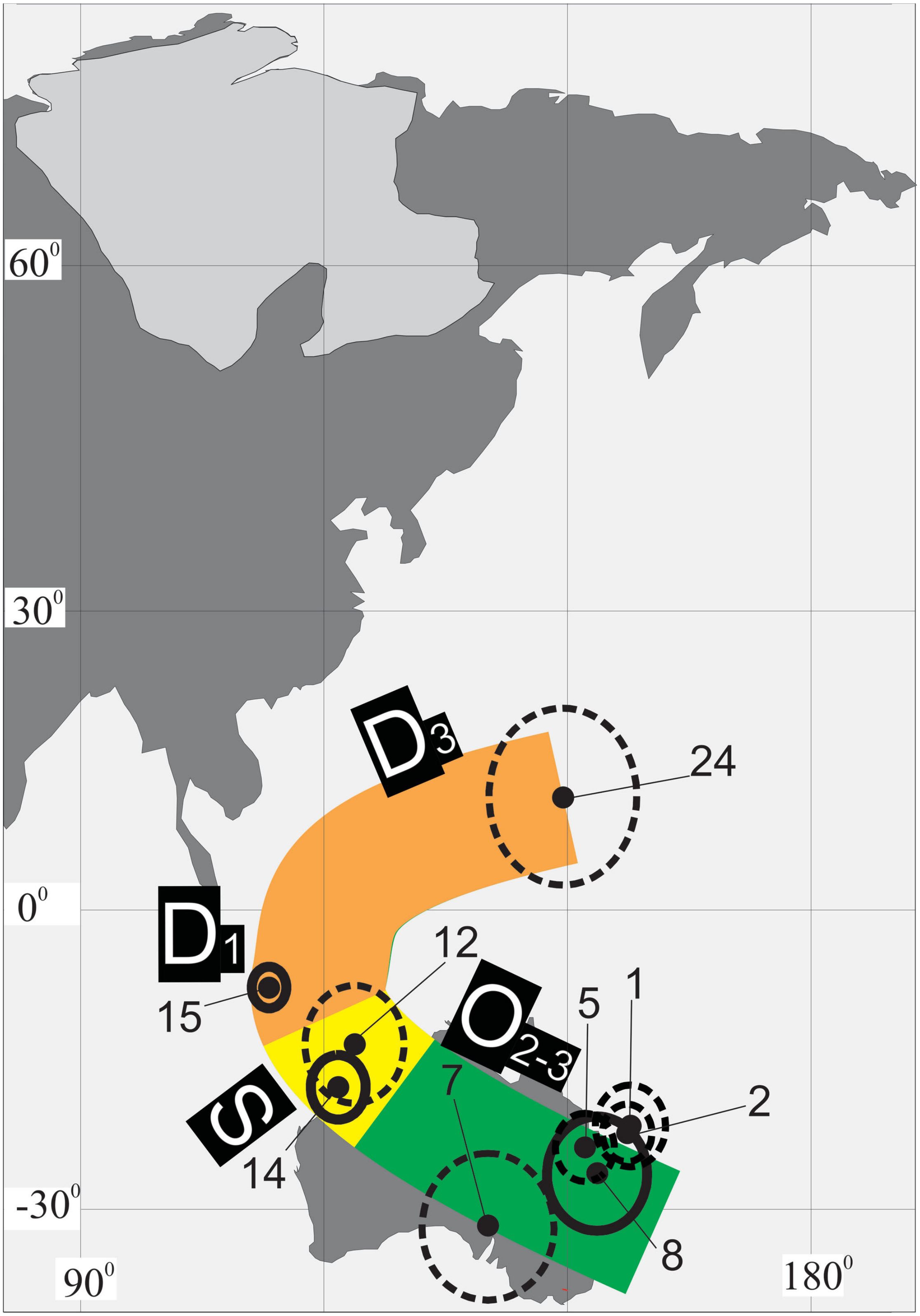

Figure 19. Palaeomagnetic poles from Angara Block for middle Ordovician–early Carboniferous. Poles from this study are corrected for Vilyuy rifting (see text).

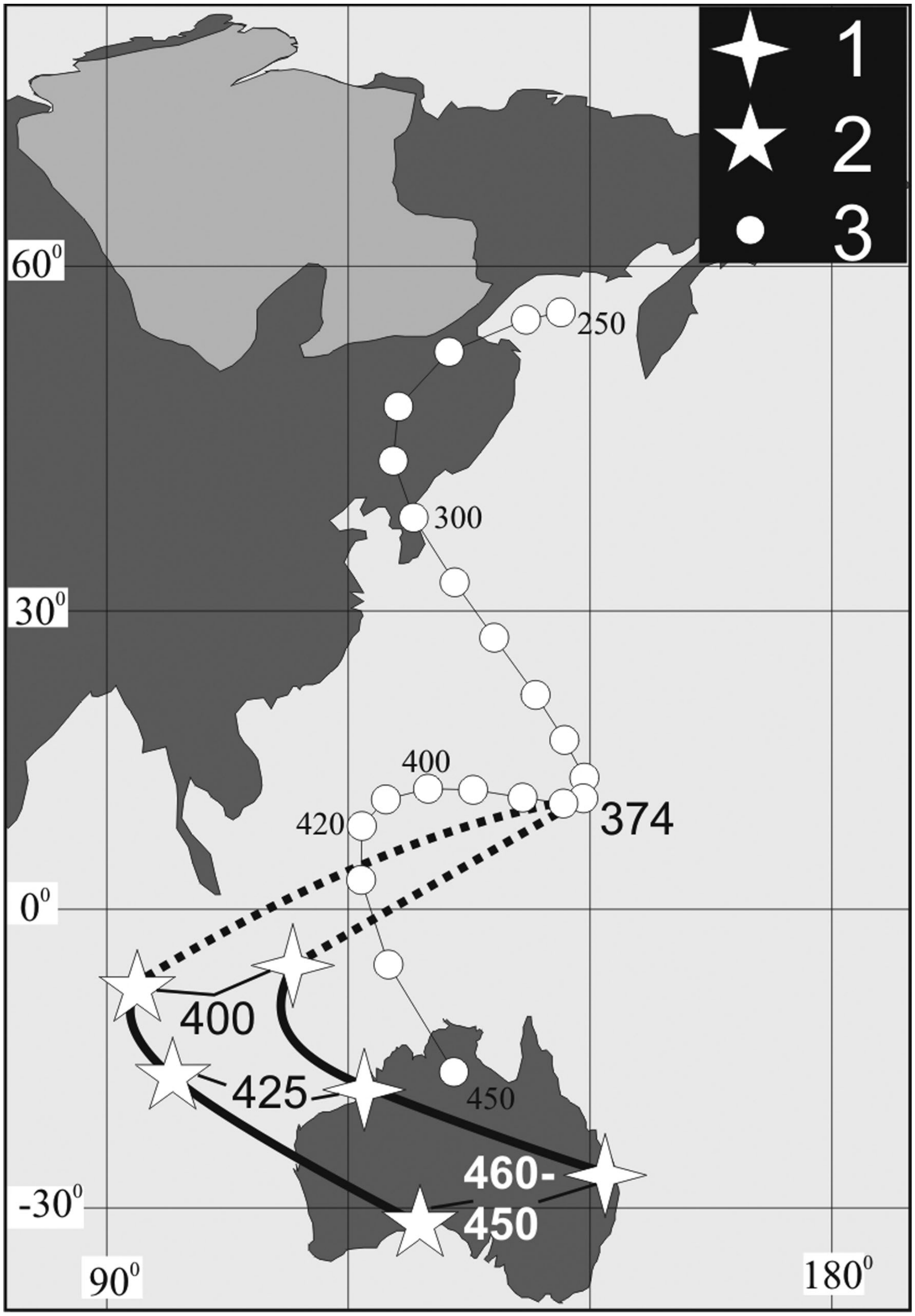

Figure 20. Middle Palaeozoic portion of Siberian APWP, 1: for the Angara block; 2: for the Aldan block; 3: spherical spline in the Angara reference frame from Cocks & Torsvik (2007).

Middle palaeozoic segment of apparent polar wander path (APWP) for the Siberian platform

The newly acquired poles help to fill in the middle Palaeozoic gap on Siberian APWP and indicate that existing versions of the Siberian APWP (i.e. Cocks & Torsvik 2007) need further elaboration. An updated version of the Siberian APWP for the middle Ordovician–early Carboniferous interval is presented in Fig. 20. We stress the necessity of using separate APWPs for the Angara and Aldan blocks for pre-Devonian poles.

Palaeogeographic implications

Based on the palaeomagnetic evidence discussed in this study, the Siberian platform was situated in periequatorial, mostly southern latitudes during the middle and late Ordovician (Fig. 21) and was rotated ∼180° about a vertical axis compared to its current orientation. The platform did not experience any significant latitudinal drift during that time. Starting in the late Ordovician, Siberia began drifting to the north. By the end of the early Silurian, the platform had travelled ∼1500 km to the north and had rotated ∼30° CCW

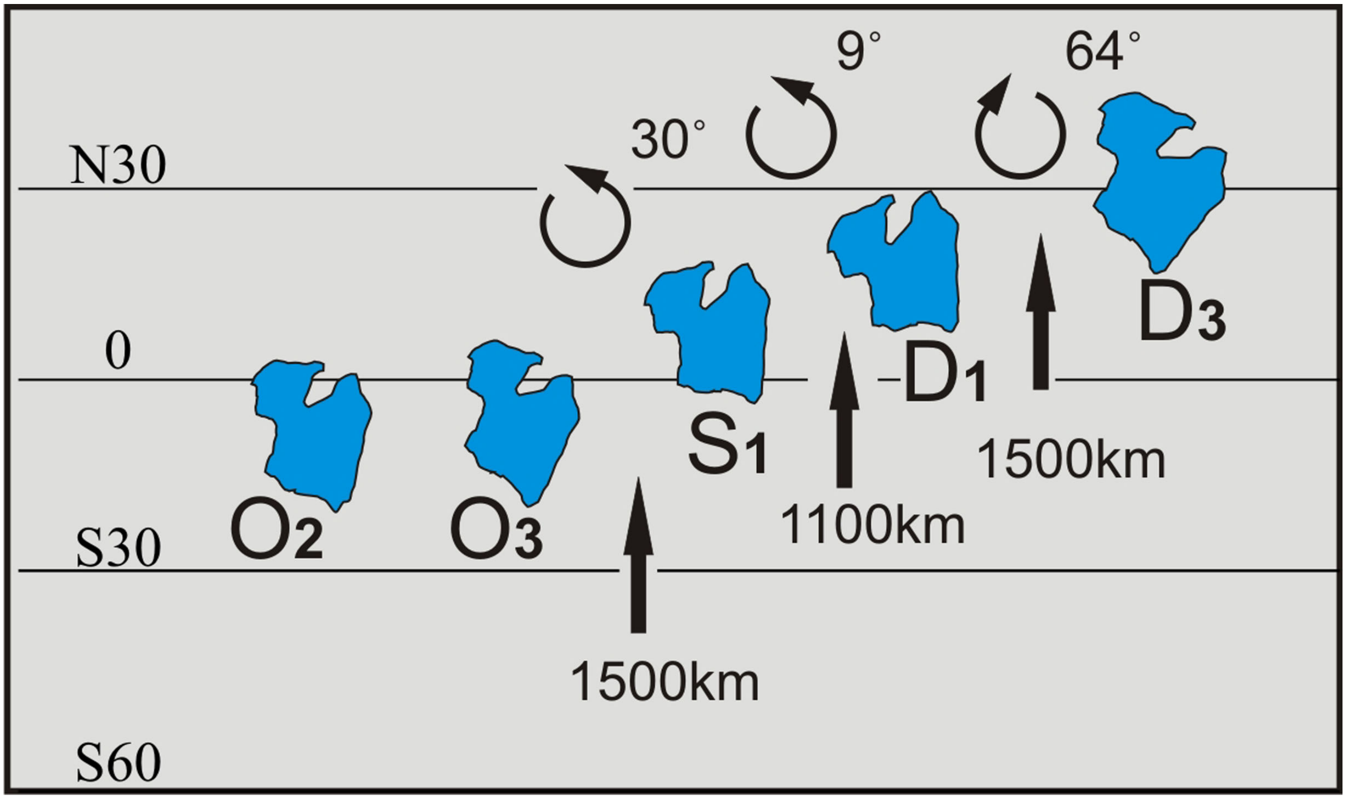

Figure 21. Palaeogeographic latitude and orientation of Siberia for late Ordovician, early Silurian and early (?) Devonian time. Straight arrows indicate northward drift, curved arrows mark rotation. The Siberian platform is shown in the post-Vilyuy-rift configuration. Late Ordovician, early Silurian and early Devonian positions have been calculated from the three isolated palaeomagnetic components. The middle Ordovician position is based on the data from Pavlov *et al.* (1999) and the late Devonian position is calculated from the pole of Kravchinsky *et al.* (2002) (age refined in Courtillot *et al.* (2010)). Palaeogeographic reconstructions in this study have been created using GMAP software (Torsvik & Smethurst 1999).

(Fig. 21). This implies an average latitudinal displacement of 5–7 cm yr^{-1}, which is high but not impossible for a continental plate. For a modern example, the Indian Plate is converging with Eurasia at a velocity reaching 6.4 cm yr^{-1} (Jade 2004).

The early Silurian pole puts the Siberian platform 10–30° more to the south compared to some previously published reconstructions (e.g. Dalziel 1997; Cocks & Torsvik 2002; Golonka *et al.* 2006; Lawver *et al.* 2011). Such a position is supported by palaeontology: the distributions of stromatoporoids (Nestor 1990), gastropods (Blodgett *et al.* 1990), rugose corals (Pedder & Oliver 1990), algae (Poncet 1990) and miospores (Streel *et al.* 1990) point towards the periequatorial position of Siberia during the mid-Palaeozoic. According to the new data, the Siberian platform continued northward drift and CCW rotation during the late Silurian, reaching ~1100 km and ~10°, respectively, by the time of the MT component, which we estimate to be early Devonian (Fig. 21). After acquisition of the MT, the rotation of the platform changed to clockwise (CW) and by late Devonian Siberia had drifted another ~1500 km to the north and had rotated ~60° CW (Fig. 21).

Palaeomagnetically permissible reconstructions of Baltica, Siberia and Laurentia are shown in Fig. 22. It is necessary to mention, however, that the palaeomagnetic method can only provide palaeolatitudes and orientations relative to the meridian. Palaeolongitudes cannot be deciphered by palaeomagnetic methods. Independent geological methods need to be employed to refine the relative positions of cratons.

In the late Ordovician, Laurentia and Baltica were at the end of their race towards each other, which ended in the Caledonian collision (e.g. Cocks & Torsvik 2005). The Siberian platform is placed to the east of Baltica in our reconstruction of Fig. 22, however, there is no palaeomagnetic prohibition against Siberia being on the western side of Laurentia instead. By mid-Silurian Baltica and Laurentia had collided during Caledonian Orogeny (Nikishin *et al.* 1996; Cocks & Torsvik 2005), forming Laurussia (or Euro-America), and in a number of palaeogeographic reconstructions for Silurian time (e.g. Torsvik *et al.* 1996; Golonka *et al.* 2003; Lawver *et al.* 2011) the Siberian platform is placed to the north of the Caledonide suture. Our data do not favour such a placement, since it could only be achieved by using the outermost parts of confidence ovals for the three cratons. Additional problems arise, taking into account the concept of middle Palaeozoic Arktida–Baltica–Laurentia composite continent (Kuznetsov 2006; Kuznetsov *et al.* 2010). According to this concept, the long-lived Arktida continent was composed of several blocks, now located all over the Arctic, the Arctic Alaska–Chukotka microplate, Novaya Zemlya, Svalbard, Novosibirsk islands and northern Taimyr, and by the Precambrian/Cambrian boundary the northeastern margin of Baltica had collided with Arktida, the two existing as a composite continent until late Mezozoic or early Cenozoic (Kuznetsov 2006). The presence of Arktida does not permit enough space for Siberia to the north of Caledonides during Silurian (see reconstruction on fig. 15A in Kuznetsov *et al.* (2010)). Thus, the most probable location

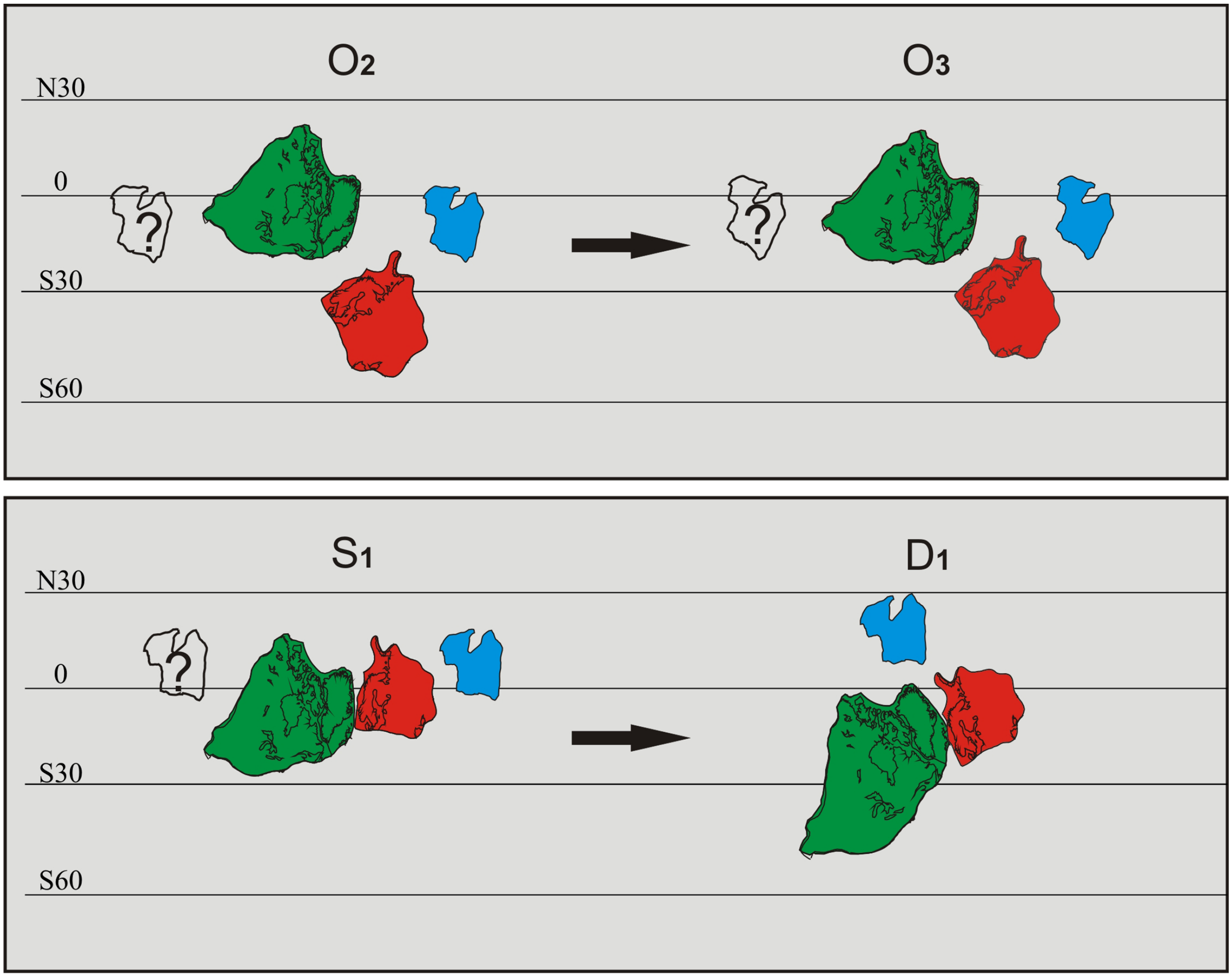

Figure 22. Palaeomagnetically viable reconstructions of Siberian (blue), Baltica (red) and Laurentian (green) platforms for the middle Ordovician–early Devonian. Longitude uncertainty in the position of Siberia is emphasized in the Ordovician and Silurian reconstructions. The Arktida continent is omitted in these reconstructions due to the absence of relevant palaeomagnetic data. Palaeomagnetic data used for the reconstructions: Laurentia*: O_2—470; O_3—450; S_1—430 and D_1—400 Ma. Baltica**: O_2—465; O_3—459; S_1—428 and D_1—400 Ma* (APWP path pole #23/24). Siberia: O_2 ***; O_3 —HT_o****; S_1—HT_s ****; D_1—MT ****.
*Spherical spline path poles, table 1 in Cocks & Torsvik (2011).
**Spherical spline path poles, table 1 in Torsvik *et al.* (1996).
***(Pavlov & Gallet 2005).
****This study.

of the Siberian platform during early Silurian was either to the east or to the west of Baltica–Laurentia(–Arktida) composite continent (Fig. 22, Arktida is not shown). The possibility of such a configuration was previously discussed by Bachtadse *et al.* (2000). Finally, the palaeomagnetic pole derived from the MT component allows 'Eurasian' position of Siberia in early Devonian (Fig. 22), compatible with the reconstructions from Torsvik *et al.* (1996), Golonka *et al.* (2003) and Lawver *et al.* (2011).

CONCLUSIONS

Our study allows us to formulate the following conclusions:

(1) Samples from the late Ordovician–Silurian sedimentary section, located in the Nyuya syncline at the south of Siberian platform document three pre-folding palaeomagnetic directions. Whereas two of them are likely to be primary, late Ordovician and early Silurian in age, the third one is a secondary overprint component.

(2) Geochronology of the folded mafic sills constrains the folding in the area to be younger than 371.0 ± 3.3 Ma, which defines the younger limit for the secondary magnetic component (MT). New geochronology data along with the age of the post-tectonic Angara–Vitim batholith confines the age of folding between 310 and 371 Ma. Based on the age of folding and on comparison with published palaeomagnetic poles for the Siberian platform, we estimate the magnetic overprint to be early Devonian, *ca.* 400 Ma, in age.

(3) The three poles calculated from our new palaeomagnetic directions for the late Ordovician, early Silurian and early Devonian help to fill in the middle Palaeozoic gap on the APWP for the Siberian platform. These data emphasize the need for further elaboration of the Siberian Palaeozoic APWP. We demonstrate the necessity of using two different APWPs for all pre-Devonian poles

for the Siberian platform, one for the Aldan Block and another for the Angara–Anabar Block, because of relative rotations of the two blocks during Vilyuy rifting.

(4) From these three new palaeomagnetic poles, we infer information about the palaeogeography of the Siberian platform (Fig. 21). In late Ordovician, the Siberian platform was located in equatorial latitudes and was rotated $\sim 180^\circ$ around a vertical axis relative to its present position. It experienced little or no northward drift or rotation between middle and late Ordovician, but by the end of the early Silurian had travelled $\sim$1500 km to the north and rotated $\sim 30^\circ$ CCW. By the early Devonian, the Siberian platform had drifted another 1100 km to the north and rotated 9° CCW, and by the end of Devonian time had drifted another 1500 km to the north and rotated $\sim 60^\circ$ CW.

(5) We present three new palaeoreconstructions of the three major platforms, Siberian, Baltica and Laurentia, for the late Ordovician, early Silurian and early Devonian (Fig. 22). The major new result is the early Silurian reconstruction, showing that the Siberian platform could not have been located to the north of the Caledonide suture zone as suggested in several reconstructions. Its place had to be either to the east or to the west of the Laurentia–Baltica–Arktida composite continent, Laurussia. By the early Devonian, however, the Siberian platform could have assumed its 'Eurasian' position.

ACKNOWLEDGEMENTS

This work was supported by the US National Science Foundation «The Siberian flood basalts and the end-Permian Extinction» (EAR-0807585); Russian Foundation for Basic Research, projects # 12-05-00403 and #07-05-00750; Russian Presidential grant #MK-139.2007.5; the programme of the RAS Division of Earth Sciences 'Geodynamic Evolution of the Lithosphere of the Central Asian Mobile Belt (from Ocean to Continent)'; the US National Science Foundation Grant EAR-0911331 and a BP fellowship in the School of Earth Sciences at Stanford University. This paper is contribution no. 509 of the Palaeomagnetism Laboratory and Center for the Study of Imaging and Dynamics of the Earth (Institute of Geophysics and Planetary Physics, University of California, Santa Cruz). We are grateful to Dr Brayshaw, a vice president of BP, for his financial help; to S. Gilder, V. Bachtadse and M. Weiss (University of Munich, Germany) for generously sharing their analytical facilities; to Pablo Garcia del Real (Stanford University) and Alex Tkach for help with manuscript revision; to Alex and Dzhumas Vereshchagins, Ivan Fedyukin and Ruslan Burnaev for help during field work; to Ilya Reznik for his help with logistics in Moscow. In Siberia, we received a considerable amount of support from the wonderful residents of Southern Nyuya Village—Boris Leontjev and Svetlana Egorova. Finally, we would like to express our gratitude to the reviewers for their input.

REFERENCES

Bachtadse, V., Pavlov, V.E., Kazansky, A.Y. & Tait, J.A., 2000. Siluro-Devonian paleomagnetic results from the Tuva Terrane (southern Siberia, Russia): implications for the paleogeography of Siberia, *J. geophys. Res.,* **105**(B6), 13 509–13 518.

Baker, J., Peate, D., Waight, T. & Meyzen, C., 2004. Pb isotopic analysis of standards and samples using a 207Pb-204Pb double spike and thallium to correct for mass bias with a double-focusing MC-ICP-MS, *Chem. Geol.,* **211**(3–4), 275–303.

Berger, A.Y., Kovalevskaya, Y.O., Tesakov, Y.I. & Khromykh, V.G., 2007. Silurian of Nyuya-Djerba and Berezov throughs, *Regionalnaya geologiya i metallogeniya (in Russian),* **30–31,** 48–56.

Blodgett, R.B., Rohr, D.M. & Boucot, A.J., 1990. Early and Middle Devonian gastropod biogeography, *Geol. Soc. Lond. Memoir,* **12,** 277–284.

Bowring, J.F., McLean, N.M. & Bowring, S.A., 2011. Engineering cyber infrastructure for U-Pb geochronology: Tripoli and U-Pb_Redux, *Geochem. Geophys. Geosyst.,* **12**(6), Q0AA19, doi:10.1029/2010GC003479.

Cocks, L.R.M. & Torsvik, T.H., 2002. Earth geography from 500 to 400 million years ago: a faunal and palaeomagnetic review, *J. geol. Soc.,* **159**(6), 631–644.

Cocks, L.R.M. & Torsvik, T.H., 2005. Baltica from the late Precambrian to mid-Palaeozoic times: the gain and loss of a terrane's identity, *Earth-Sci. Rev.,* **72,** 39–66.

Cocks, L.R.M. & Torsvik, T.H., 2007. Siberia, the wandering northern terrane, and its changing geography through the Palaeozoic, *Earth-Sci. Rev.,* **82,** 29–74.

Cocks, L.R.M. & Torsvik, T.H., 2011. The Palaeozoic geography of Laurentia and western Laurussia: a stable craton with mobile margins, *Earth-Sci. Rev.,* **106**(1–2), 1–51.

Courtillot, V., Kravchinsky, V.A., Quidelleur, X., Renne, P.R. & Gladkochub, D.P., 2010. Preliminary dating of the Viluy traps (Eastern Siberia): eruption at the time of Late Devonian extinction events? *Earth planet. Sci. Lett.,* **300**(3–4), 239–245.

Dalziel, I.W.D., 1997. Overview: Neoproterozoic-Paleozoic geography and tectonics: review, hypothesis, environmental speculation, *Geol. Soc. Am. Bull.,* **109**(1), 16–42.

Debiche, M.G. & Watson, G.S., 1995. Confidence limits and bias correction for estimating angles between directions with applications to paleomagnetism, *J. geophys. Res.,* **100,** 24 405–24 430.

DeBoisgrollier, T., Petit, C., Fournier, M., Leturmy, P., Ringenbach, J.-C., San'kov, V.A., Anisimova, S.A. & Kovalenko, S.N., 2009. Palaeozoic orogeneses around the Siberian craton: structure and evolution of the Patom belt and foredeep, *Tectonics,* **28**(1), TC1005, doi:10.1029/2007TC002210.

Didenko, A.N., Mossakovsky, A.A., Pechersky, D.M., Ruzhentsev, S.V., Samygin, S.G. & Heraskova, T.N., 1994. Geodynamics of Paleozoics Oceans of Central Asia, *Russ. geol. Geophys.,* **35,** 59–75.

Eide, E.A. & Torsvik, T.H., 1996. Paleozoic supercontinental assembly, matle flushing, and genesis of the Kiaman Superchron, *Earth planet. Sci. Lett.,* **144**(96), 389–402.

Enkin, R.J., 1994. A computer program package for analysis and presentation of palaeomagnetic data, *Pacific Geoscience Centre, Geological Survey of Canada,* 16pp.

Fisher, R., 1953. Dispersion on a sphere, *Proc. R. Soc. A,* **217**(1130), 295–305.

Gallet, Y. & Pavlov, V.E., 1996. Magnetostratigraphy of the Moyero river section (north-western Siberia): constraints on geomagnetic reversal frequency during the early Palaeozoic, *Geophys. J. Int.,* **125,** 95–105.

Gerstenberger, H. & Haase, G., 1997. A highly effective emitter substance for mass spectrometric Pb isotope ratio determinations, *Chem. Geol.,* **136,** 309–312.

Golonka, J., Bocharova, N., Ford, D., Edrich, M., Bednarczyk, J. & Wildharber, J., 2003. Paleogeographic reconstructions and basins development of the Arctic, *Mar. Petrol. Geol.,* **20,** 211–248.

Golonka, J., Krobicki, M., Paul, Z. & Khudoley, A.K., 2006. Central Asia–Southeast Asia connection during Paleozoic orogenies: problems and questions, in *Structural and tectonic correlation across the Central Asian Orogenic Collage: implications for continental growth and intracontinental deformation: Second International Workshop and Field Excursions for IGC Project-480,* Ulaanbaatar, Mongolia, pp. 21–23.

Irving, E. & Parry, L.G., 1963. The magnetism of some Permian rocks from New South Wales, *Geophys. J. R. astr. Soc.,* **7,** 395–411.

Jade, S., 2004. Estimates of plate velocity and crustal deformation in the Indian subcontinent using GPS geodesy, *Curr. Sci.,* **86**(10), 1443–1448.

Khain, V.E., 2001. *Tectonics of Continents and Oceans (year 2000)*, Nauchnyi Mir (in Russian), Moscow, 606pp.

Khramov, A.N., 1958. *Paleomagnetism and Stratigraphic Correlation,* Gostoptechizdat, Leningrad, 218pp. (English transl, published by School of Earth Sciences, Australian National University, Canberra, Australia.)

Khramov, A.N., 1967. The Earth's magnetic field in the late Paleozoic, *Akad. Nauk S.S.R. Izv. Earth Phys. Ser.,* 86–108.

Khramov, A.N., 1974. *Paleomagnetism of the Paleozoic,* Nedra, Leningrad.

Kirschvink, J.L., 1980. The least-squares line and plane and the analysis of palaeomagnetic data, *Geophys. J. R. astr. Soc.,* **62,** 699–718.

Kravchinsky, V.A., Konstantinov, K.M., Courtillot, V., Savrasov, J.I., Valet, J.-P., Cherniy, S.D., Mishenin, S.G. & Parasotka, B.S., 2002. Palaeomagnetism of East Siberian traps and kimberlites: two new poles and palaeogeographic reconstructions at about 360 and 250 Ma, *Geophys. J. Int.,* **148,** 1–33.

Krogh, T.E., 1972. A low-contamination method for hydrothermal decomposition of zircon and extraction of U and Pb for isotopic age determinations, *Geochim. cosmochim. Acta,* **37,** 485–494.

Kuznetsov, N.B., 2006. The Cambrian Baltica-Arctida collision, pre-Uralide-Timanide orogen, and its erosion products in the Arctic, *Doklady Earth Sci.,* **411**(2), 1375–1380.

Kuznetsov, N.B., Natapov, L.M., Belousova, E.A., Reilly, S.Y.O. & Griffin, W.L., 2010. Geochronological, geochemical and isotopic study of detrital zircon suites from late Neoproterozoic clastic strata along the NE margin of the East European Craton: implications for plate tectonic models, *Gondwana Res.,* **17**(2–3), 583–601.

Lawver, L.A., Gahagan, L.M. & Norton, I., 2011. Palaeogeographic and tectonic evolution of the Arctic region during the Palaeozoic, in *Arctic Petroleum Geology,* Vol. 35, pp. 61–77, eds Spenger, A.M., Embry, A.F., Gautier, D.L., Stoupakova, A.V. & Sorensen, K.,Geological Society, London, Memoirs.

Ludwig, K.R., 2001. SQUID 1.02, A User's Manual, Berkeley Geochronology Center, Special Publication, **2,** 1–21.

Masaitis, V.L., Mikhailov, M.V. & Staritsky, Y.G., 1975. *Volcanism and Tectonics of Patom-Vilyuy Middle Paleozoic aulacogen (in Russian),* Nedra, Moscow.

Mattinson, J.M., 2005. Zircon U–Pb chemical abrasion ('CA-TIMS') method: combined annealing and multi-step partial dissolution analysis for improved precision and accuracy of zircon ages, *Chem. Geol.,* **220**(1–2), 47–66.

McFadden, P.L. & McElhinny, M.W., 1990. Classification of the reversal test in palaeomagnetism, *Geophys. J. Int.,* **103**(3), 725–729.

McLean, N.M., Bowring, J.F. & Bowring, S.A., 2011. An algorithm for U-Pb isotope dilution data reduction and uncertainty propagation, *Geochem. Geophys. Geosyst.,* **12**(6), Q0AA18, doi:10.1029/2010GC003478.

Mikhailov, M.V., 1974. *USSR State Geological Map (and Explanatory Note), Scale 1:200 000, Sheet R-50-XXVII,* Moscow.

Mikhailov, M.V. & Timofeev, S.A., 1978. *USSR State Geological Map (and Explanatory Note), Scale 1:200 000, Sheet R-50-XXVI,* Moscow.

Nestor, H., 1990. Biogeography of Silurian stromatoporoids, *Geol. Soc. Lond. Memoir,* **12,** 215–221.

Nikishin, A.M. *et al.*, 1996. Late Precambrian to Triassic history of the East European Craton: dynamics of sedimentary basin evolution, *Tectonophysics,* **268**(1–4), 23–63.

Nikishin, A.M., Sobornov, K.O., Prokopiev, A.V. & Frolov, S.V., 2010. Tectonic evolution of the Siberian Platform during the Vendian and Phanerozoic, *Mosc. Univ. geol. Bull.,* **65**(1), 1–16.

Nikolsky, F.V. & Kavelin, Y.I., 1984. *USSR State Geological Map (and Explanatory Note), Scale 1:200 000, Nyuya Sheet (R-50-XXXIII),* Moscow.

Parfenov, L.M., 2001. *Tectonics, Geodynamics, and Metallogeny of the Territory of the Sakha Republic (Yakutia) (in Russian),* Nauka/Inte., eds Parfenov, L.M. & Kuzmin, M.I., MAIK "Nauka"/Interperiodika, Moscow.

Pavlov, V.E., 2012. Siberian paleomagnetic data and the problem of rigidity of the northern Eurasian Continent in the post Paleozoic, *Izv. Phys. Solid Earth,* **48**(9–10), 721–737.

Pavlov, V.E. & Gallet, Y., 2005. A third superchron during the Early Paleozoic, *Episodes,* **28**(2), 1–7.

Pavlov, V.E., Bachtadse, V. & Mikhailov, V., 2008. New Middle Cambrian and Middle Ordovician palaeomagnetic data from Siberia: Llandelian magnetostratigraphy and relative rotation between the Aldan and Anabar–Angara blocks, *Earth planet. Sci. Lett.,* **276**(3–4), 229–242.

Pavlov, V.E., Courtillot, V., Bazhenov, M.L. & Veselovsky, R.V., 2007. Paleomagnetism of the Siberian traps: new data and a new overall 250 Ma pole for Siberia, *Tectonophysics,* **443**(1–2), 72–92.

Pavlov, V.E., Rodionov, V.P., Khramov, A.N. & Gallet, Y., 1999. Magnetostratigraphy of the Polovinka key section, midstream Lena River: did the geomagnetic polarity change in the Early Llandeilian? *Izv. Phys. Solid Earth,* **35**(5), 402–412.

Pavlov, V.E., Veselovskiy, R.V., Shatsillo, A.V & Gallet, Y., 2012. Magnetostratigraphy of the Ordovician Angara/Rozhkova River section: further evidence for the Moyero reversed superchron, *Izv. Phys. Solid Earth,* **48**(4), 297–305.

Pedder, A.E.H. & Oliver, W., 1990. Rugose coral distribution as a test of Devonian palaeogeographic models, *Geol. Soc. Lond. Memoir,* **12,** 267–275.

Poncet, J., 1990. Biogeography of Devonian algae, *Geol. Soc. Lond. Memoir,* **12,** 285–289.

Rodionov, V.P., Osipova, E.P. & Pogarskaya, I.A., 1982. Pole #10023, in *Paleomagnetic Directions and Paleomagnetic Poles: Data for the USSR, Issue 5 (in Russian),* Moscow.

Rodionov, V.P., Dekkers, M.J., Khramov, A.N., Gurevitch, E.L., Krugsman, W., Duermeijer, C.E. & Heslop, D., 2003. Paleomagnetism and cyclostratigraphy of the Middle Ordovician Krivolutsky suite, Krivaya Luka section, southern Siberian Platform: record of non-synchronous NRM-components or a non-axial geomagnetic field, *Stud. Geophys. Geod.,* **47,** 255–274.

Shatsillo, A.V., 2005. Reconnaissance paleomagnetic study of igneous rocks in the Sharyzhalgaiskii Inlier of the Siberian Craton in the confluence area of the B. Zhidoi and Toisuk rivers, in *Structure of the Lithosphere and Geodynamics,* pp. 255–258, Irkutsk.

Shatsillo, A.V., Fedyukin, I.V. & Powerman, V.I., 2013. Palaeomagnetism of Late Palaeozoic granitoids of Angara-Vitim Batholith and host rocks of Baikal-Patom fold belt: tectonic consequences, *Geol. Geofiz. (in Russian),* in press.

Shatsillo, A.V., Konstantinov, K.M. & Kochnev, B.B., 2004. Stages, genesis, and timing of formation of Baikal-Patom arc folded structure based on palaeomagnetic data, in *Youth School-Conference of the XXXVII Tectonic Meeting 'Evolution of tectonic processes in Earth's history',* pp. 113–120, GEOS, Moscow.

Shatsillo, A.V., Powerman, V.I. & Pavlov, V.E., 2007. Middle Paleozoic segment of the apparent polar wander path from the Siberian platform: new paleomagnetic evidence for the Silurian of the Nyuya-Berezovskii facial province, *Fiz. Zemli (in Russian),* **43**(10), 85–94.

Shipitsin, A.D. & Shipitsina, L.V., 1971. *USSR State Geological Map (and Explanatory Note), Scale 1:200 000, Iskra sheet (R-50-XXXII),* Leningrad, Russia.

Smethurst, M.A., Khramov, A.N. & Torsvik, T.H., 1998. The Neoproterozoic and Palaeozoic palaeomagnetic data for the Siberian platform: from Rodinia to Pangea, *Earth Sci. Rev.,* **43,** 1–24.

Streel, M., Fairon-Demaret, M. & Loboziak, S., 1990. Givetian-Frasnian phytogeography of Euramerica and western Gondwana based on miospore distribution, *Geol. Soc. Lond. Memoir,* **12,** 291–296.

Tan, X. & Kodama, K.P., 2003. An analytical solution for correcting palaeomagnetic inclination error, *Geophys. J. Int.,* **152**(1), 228–236.

Tauxe, L. & Kent, D.V., 2004. A simplified statistical model for the geomagnetic field and the detection of shallow bias in paleomagnetic inclinations: was the ancient magnetic field dipolar? in *Timescales of the Paleomagnetic Field*, Geophysical Monograph Series, Vol. 145, pp. 101–115, eds Channell, J.E.T., Kent, D.V., Lowrie, W. & Meert, J.G.

Torsvik, T.H. & Smethurst, M.A., 1999. Plate tectonic modelling: virtual reality with GMAP, *Comput. Geosci.,* **25,** 395–402.

Torsvik, T.H., Tait, J.A., McKerrow, W.S., Sturt, B.A. & Roberts, D., 1995. Ordovician palaeogeography of Siberia and adjacent continents,, *J. geol. Soc.,* **152,** 279–287.

Torsvik, T.H., Smethurst, M.A., Meert, J.G., VanDerVoo, R., McKerrow, W.S., Brasier, M.D., Sturt, B.A. & Walderhaug, H.J., 1996. Continental break-up and collision in the Neoproterozoic and Palaeozoic: a tale of Baltica and Laurentia, *Earth-Sci. Rev.,* **40,** 229–258.

Tsygankov, A.A., Matukov, D.I., Berezhnaya, N.G., Larionov, A.N., Posohov, V.F., Tsyrenov, B.T., Hromov, A.A. & Sergeev, S.A., 2007. Late Paleozoic granitoids of western Transbaikalia: magma sources and stages of formation, *Geol. Geofiz. (in Russian),* **48**(1), 156–180.

Williams, I.S., 1998. U-Th-Pb geochronology by ion microprobe: not just ages but histories, in *Applications of Microanalytical Techniques to Understanding Mineralizing Processes,* Reviews in Economic Geology, pp. 1–35, eds McKibben, M.A., Shanks, W.C. & Ridley, W.I., *Society of Economic Geologists*

Windley, B.F., Alexeiev, D., Xiao, W., Kroner, A. & Badarch, G., 2007. Tectonic models for accretion of the Central Asian Orogenic Belt, *J. geol. Soc. Lond.,* **164**(2004), 31–47.

Xiao, W., Windley, B.F., Hao, J. & Zhai, M., 2003. Accretion leading to collision and the Permian Solonker suture, Inner Mongolia, China: termination of the central Asian orogenic belt, *Tectonics,* **22**(6), 1069, doi:10.1029/2002TC001484.

Zarubin, A.S., 1978. *USSR State Geological Map (and Explanatory Note), Scale 1:200 000, Sheet R-50-XXV,* Moscow.

Zonenshain, L.P., Kuzmin, M.I. & Natapov, L.M., 1990. *Geology of the USSR: A Plate-Tectonic Synthesis,* ed. Page, B.M., American Geophysical Union.

APPENDIX A: PALAEONTOLOGICAL FOSSILS IN LATE ORDOVICIAN–SILURIAN ROCKS OF THE NYUYA SYNCLINE

APPENDIX B: SAMPLING, PROCESSING AND ANALYTICAL GEOCHRONOLOGY PROCEDURES; COMPLETE GEOCHRONOLOGICAL DATA TABLES FOR TWO GABBROIC BODIES

The two collected samples were processed and analysed in different laboratories using different methods.

Sample VP-VI-Le-1 was mechanically crushed and ground, then hand-sieved. Strongly magnetic grains were removed using a hand magnet. The rest of material was processed in heavy liquids (methylene iodide). The heavy fraction was run on a sloped Frantz magnetometer. Zircons were handpicked using reflected and transmitted light. U-Pb isotopic analyses were carried out by isotope dilution-thermal ionization mass spectrometry (ID-TIMS) at the Massachusetts Institute of Technology (MIT). Zircons for U-Pb dating were dissolved using the chemical abrasion method (Mattinson 2005), modified for single grain dating. Prior to dissolution, zircons were annealed at 900 °C for 48 hr. Individual grains were then loaded into teflon microcapsules with 29 N HF, placed in Parr acid digestion vessels, and leached at 180–210 °C for 12–14 hr. Each leached grain was subsequently transferred to a clean teflon beaker for rinsing. Following removal of the HF solution, grains were rinsed in H_2O, placed in an ultrasonic for 15–20 min in ∼7 N HNO_3, fluxed on a hot plate for 1 hr in ∼7 N HNO_3, and then rerinsed in H_2O prior to loading. The rinsed grains were loaded into cleaned teflon microcapsules, spiked with the EARTHTIME ^{205}Pb-^{233}U-^{235}U tracer (ET535) and dissolved in ∼29 N HF in Parr acid

Table A1. Faunal remains in the study sedimentary section. Data compiled from Berger *et al.* (2007), Mikhailov & Timofeev (1978), Mikhailov (1974), Zarubin (1978), Nikolsky & Kavelin (1984) and Shipitsin & Shipitsina (1971).

Neryukteiskaya formation:
None
Nyuiskaya formation:
Brachiopods: Hyattidina parva (Nikif.), Lenatoechia sp.
Conodonts: Ozarkodina tamashkovae Mosk., Panderodus unicostatus (Bran. et Mehl.).
Gastropods: Hormotoma gracilis Gub., Murchisonia *cf.* singulata (Hising.), Straparollus *cf.* alacer Pern.; Trochonema transformis Gub., Loxoplocus sp.
Ostracods: Hogmochilina *cf.* maaki (F. Schmidt)
Orthoceratidaes: Armenoceras bachtense Balash., Huroniella inflecta (Parks).
Stromatoporata: Yavorskiina aspectabilis (Yavor.), Clavidictyon cylindricum (Yavor.), Ecclimadictyon fastigiatum (Nich.)
Tabulate corals: Favosites gothlandicus moyeroensis Sok. et Tes., Sapporipora favositoides Ozaki, Subalveolites subulosus Sok. et Tes.
Tentaculites: Costatulites sp.
Utakanskaya formation:
Bivalves: Modiolopsis sp.
Brachiopods: Lenatoechia elegans (Nikif.), Fardenia *cf.* gorbiyatchensis (Lop.).
Conodonts: Acodus curvatus Brans. et Mehl., Distomodus kentuckyensis Brans. et Brans. (in the lower part of the formation), Oulodus kentuckyensis (Brans. et Brans.)
Crinoideas: Bazaricrinus angularis Stuk., Glyptocrinus sp., Tajmirocrinus sp.
Fishes: Elegestolepis conica Kar.-Tal., Loganellia sibirica Kar.-Tal., L. moskalenkoae Kar.-Tal.
Ostracods: Herrmannina sp., Hogmochilina sp.
Tabulate corals: Favosites gothlandicus Lam.
Melichanskaya formation
Brachiopods: Lenatoechia elegans (Nikif.), Septatrypa *cf.* pentagonalis Nikif., Stegerhynchus sp., Zygospiraella sp.
Conodonts: Distomodus kentuckyensis Brans. et Brans., Icriodella discreta Poll., Rexr. et Nic., Ozarcodina oldhamensis (Rexr.), O. nassi (Poll., Rexr. et Nic.), Panderodus sp.,
Ostracods: Hogmochilina *cf.* elongata Abush.
Pelecypodas genus: Modiolopsis and Bacaloidea
Tabulate corals: Favosites gothlandicus Lam.
Telodonts: Distomodus kentuckyensis Brans. et Brans., Icriodella discreta Poll., Rexr. et Nic., Ozarcodina oldhamensis (Rexr.), O. nassi (Poll., Rexr. et Nic.), Panderodus sp.
Krasnokamenskaya formation
Conodonts: Drepanodistacodus victrix Mosk., Acanthodina regalis Mosk.

Table B1. U-Th-Pb isotopic data for sample VP-VI-Le-1.

Fraction	Composition: Th/U (a)	Composition: Pb* (b) [pg]	Composition: Pbc *(c) [pg]	Composition: Pb*/Pbc (d)	Isotopic Ratios: $^{206}Pb/^{204}Pb$ (e)	Isotopic Ratios: $^{206}Pb/^{238}U$ (f,g)	±1σ [%]	Isotopic Ratios: $^{207}Pb/^{235}U$ (f)	±1σ [%]	Isotopic Ratios: $^{207}Pb/^{206}Pb$ (f,g)	±1σ [%]	Dates (Ma): $^{206}Pb/^{238}U$ (g,h)	±1σ [abs.]	Dates (Ma): $^{207}Pb/^{235}U$ (h)	±1σ [abs.]	Dates (Ma): $^{207}Pb/^{206}Pb$ (g,h)	±1σ [abs.]	Corr. coef.
VP-VI-Le-1:																		
Zircon																		
z1	0.86	53.6	0.38	140.93	7753.7	0.060346	0.03	0.45024	0.07	0.054137	0.052	377.731	0.105	377.449	0.22	375.72	1.15	0.71
z2	0.82	23.9	1.66	14.39	815.8	0.060601	0.09	0.45313	0.37	0.054255	0.348	379.277	0.311	379.468	1.18	380.63	7.80	0.40
z4	0.93	40.6	0.44	91.40	4959.1	0.060430	0.04	0.45104	0.11	0.054157	0.079	378.238	0.130	378.006	0.35	376.59	1.75	0.91
z5	0.94	22.3	0.41	54.95	2980.2	0.060500	0.05	0.45133	0.16	0.054129	0.121	378.665	0.167	378.210	0.49	375.42	2.70	0.78
z6	0.92	65.1	0.65	99.81	5419.3	0.060404	0.05	0.45065	0.09	0.054134	0.083	378.080	0.177	377.736	0.26	375.63	1.90	0.28
z10	0.84	61.4	0.75	81.96	4542.6	0.060353	0.03	0.45121	0.09	0.054247	0.068	377.772	0.104	378.128	0.29	380.31	1.70	0.63
z11	0.77	15.8	0.26	60.62	3417.0	0.060550	0.07	0.45260	0.14	0.054236	0.116	378.971	0.238	379.095	0.45	379.85	2.70	0.54
z12	0.73	22.2	0.29	76.10	4329.1	0.060332	0.03	0.45060	0.09	0.054191	0.070	377.646	0.101	377.696	0.28	378.00	1.75	0.52
z14	1.02	30.2	0.24	127.05	6734.3	0.060430	0.04	0.45078	0.09	0.054126	0.056	378.239	0.156	377.824	0.28	375.28	1.45	0.73

Blank composition: 206Pb/204Pb = 18.41 ± 0.24; 207Pb/204Pb = 15.41 ± 0.15; 208Pb/204Pb = 37.61 ± 0.56

(a) Th contents calculated from radiogenic 208Pb and the 207Pb/206Pb date of the sample, assuming concordance between U-Th and Pb systems. (b) Total mass of radiogenic Pb.

(c) Total mass of common Pb.

(d) Ratio of radiogenic Pb (including 208Pb) to common Pb.

(e) Measured ratio corrected for fractionation and spike contribution only.

(f) Measured ratios corrected for fractionation, tracer, blank and initial common Pb.

(g) Corrected for Initial Th/U disequilibrium using radiogenic 208Pb and Th/U [magma] = 2.8

(h) Isotopic dates calculated using the decay constants λ238 = 1.55125E-10, λ235 = 9.8485E-10 (Jaffey et al. 1971), and for the 238U/235U = 137.818 ± 0.045 (Hiess, J. et al. 2012)

Table B2. U-Th-Pb isotopic data for sample VP-VII-Mu-1.

Fraction	Composition: % $^{206}Pb_c$	Composition: ppm U	Composition: ppm Th	Composition: $^{232}Th/^{238}U$	ppm $^{206}Pb^*$	Isotopic Ratios: Total $^{238}U/^{206}Pb$	±1σ[%]	Isotopic Ratios: Total $^{207}Pb/^{206}Pb$	±1σ[%]	Isotopic Ratios: $^{238}U/^{206}Pb^{*(1)}$	±1σ[%]	Isotopic Ratios: $^{207}Pb^*/^{206}Pb^{*(1)}$	±1σ[%]	Isotopic Ratios: $^{207}Pb^*/^{235}U^{(1)}$	±1σ[%]	Isotopic Ratios: $^{206}Pb^*/^{238}U^{(1)}$	±1σ[%]	err.corr	Dates (Ma): $^{206}Pb/^{238}U^{(1)}$	±1σ[abs]	Dates (Ma): $^{206}Pb/^{238}U^{(2)}$	±1σ[abs]	Dates (Ma): $^{206}Pb/^{238}U^{(3)}$	±1σ[abs]	Dates (Ma): $^{207}Pb/^{206}Pb^{(1)}$	±1σ[abs]	%Discordant
VP-VII-Mu-1: Zircon																											
1.1	-0.02594	2209.60027	5575.47305	2.60724	109	17.358	0.42	0.05451	1.00	17.353	0.41	0.05472	1.0	0.4348	1.1	0.05763	0.41	0.37015	361.2	1.4	360.7	1.50	371.8	3.1	401	23	11.01022
2.1	0.29553	3521.83815	17657.95860	5.18064	178	16.991	0.42	0.05413	0.79	17.041	0.45	0.0517	2.6	0.419	2.6	0.05868	0.45	0.17045	367.6	1.6	368.6	1.50	431	16.0	274	59	-25.46887
3.1	0.17083	2320.92785	5942.57847	2.64561	118	16.874	0.47	0.05358	0.98	16.903	0.50	0.0522	2.8	0.426	2.9	0.05916	0.50	0.17584	370.5	1.8	371.3	1.70	384.4	3.4	294	64	-20.65964
4.1	0.08115	1436.56385	3381.30409	2.43205	73.3	16.832	0.48	0.0537	1.30	16.846	0.49	0.05305	1.8	0.4342	1.8	0.05936	0.49	0.26758	371.7	1.8	372.2	1.80	384.4	3.5	331	40	-11.00196
5.1	0.14516	2077.22454	3731.70481	1.85625	104	17.126	0.49	0.05448	1.00	17.151	0.51	0.0533	2.2	0.4286	2.2	0.0583	0.51	0.22613	365.3	1.8	365.6	1.80	372.6	2.7	342	50	-6.34867
6.1	0.05243	2899.11377	2151.43214	0.76679	148	16.877	0.38	0.05391	0.88	16.886	0.38	0.05349	1.0	0.4367	1.1	0.05922	0.38	0.35739	370.9	1.4	371.1	1.40	371.9	1.6	350	23	-5.73344
7.1	0.07114	3289.40723	4921.14254	1.54583	169	16.69	0.37	0.05408	0.82	16.701	0.37	0.05351	1.3	0.4417	1.4	0.05987	0.37	0.26694	374.9	1.4	375.1	1.40	383.3	1.9	350	30	-6.56000
8.1	0.04604	1364.60827	2759.97272	2.08982	67.8	17.279	0.49	0.05522	1.30	17.287	0.49	0.05484	1.5	0.4374	1.5	0.05785	0.49	0.31940	362.5	1.7	362.1	1.80	367	2.9	406	33	11.96127

Pb_c and Pb^* indicate the common and radiogenic portions, respectively.

Error in Standard calibration was 0.43%(not included in above errors but required when comparing data from different mounts).

(1) Common Pb corrected using measured ^{204}Pb.

(2) Common Pb corrected by assuming $^{206}Pb/^{238}U$-$^{207}Pb/^{235}U$ age-concordance

(3) Common Pb corrected by assuming $^{206}Pb/^{238}U$-$^{208}Pb/^{232}Th$ age-concordance

digestion vessels held at 210 °C for 48 hr. Following the digestion, sample solutions were converted to 6.2 N HCl, then 3.1 N HCl, and U and Pb were separated via anion exchange columns (Krogh 1972). U and Pb Isotopic analyses were carried out on a VG sector 54 TIMS. Samples were loaded in silica gel (Gerstenberger & Haase 1997) onto outgassed Re filaments. Pb isotopes were measured by peak-hopping on the Daly detector and fractionation corrected based on repeat analyses of NBS 981 using the isotopic composition of Baker *et al.* (2004). U isotopes were measured statically on Faraday cups and fractionation corrected using the ^{233}U-^{235}U double spike. All measured ^{204}Pb was assumed to be from laboratory blank, which was subtracted using Pb isotopic ratios determined by repeat analyses of spiked total procedural blanks. All data reduction and error propagation was done using the U-Pb Redux software package (Bowring *et al.* 2011; McLean *et al.* 2011). ^{206}Pb/^{238}U and ^{207}Pb/^{206}Pb ratio were corrected for initial exclusion of ^{230}Th from the ^{238}U decay chain using the model Th/U of the zircon, calculated from the ^{208}Pb/^{206}Pb.

Sample VP-VII-Mu-1: Following identical methods of the other sample, zircons were mounted onto epoxy resin along with the TEMORA and 91500 standards for the Pb/U age calibration. Zircons were imaged with reflected light, transmitted light and cathodoluminiscence to identify possible overgrowths and cores. U-Pb dating of the zircons was conducted on SHRIMP-II (sensitive high-resolution ion microprobe) at the VSEGEI Institute (Saint-Petersburg, Russia). Employed procedures were similar to the ones discussed in Williams (1998). The intensity and the diameter of the primary oxygen ionic beam equalled 2 nA and 35 μm, respectively. Data reduction was done with the SQUID software (Ludwig 2001).